Turning the tide: comparison of tidal flow by periodic sealevel fluctuation and by periodic bed tilting in the Metronome tidal facility

Maarten G. Kleinhans[1], Maarten van der Vegt[1], Jasper Leuven[1], Lisanne Braat[1], Henk Markies[1], Arjan Simmelink[2], Chris Roosendaal[1], Arjan van Eijk[1], Paul Vrijbergen[1], and Marcel van Maarseveen[1]

[1]Faculty of Geosciences, Utrecht University, PObox 80115, 3508 TC Utrecht, The Netherlands
[2]Consmema design and steel construction, Hattem, The Netherlands

Correspondence to: M.G. Kleinhans, m.g.kleinhans@uu.nl

Abstract. Analogue models or scale experiments of estuaries and short tidal basins are notoriously difficult to create in the laboratory because of the difficulty to obtain currents strong enough to transport sand. Since Osborne Reynolds' experiments over a century ago, experimental tidal flow has been driven by periodic sealevel fluctuations. Recently we discovered a novel method to drive periodic tidal currents: periodically tilting the entire flume. This leads to sediment transport in both the ebb

5 and flood phase which in tidal systems with dynamic channel and shoal patterns. Here we compare the tidal currents driven by sealevel fluctuations with those driven by tilting. We use a bespoke flume of 20 m by 3 m with rough bed: the Metronome. Experiments were run in a straight flume with different tilting periods and with either one or both boundaries open at constant head with free inflow and outflow. Also experiments were run with flow driven by periodic sealevel fluctuations. We recorded surface flow velocity along the flume with Particle Imaging Velocimetry and water levels along the flume. Furthermore we

10 compared the results to a one-dimensional model with shallow flow equations for a rough bed. We found that Reynolds' method results in negligible flows along the flume except for the first few meters, whereas flume tilting results in nearly uniform, reversing flow velocities along the entire flume that are strong enough to move sand. A periodically tilting flume therefore has the potential to simulate estuaries as observed in a pilot experiment and opens up the possibility of systematic biomorphological experimentation with self-formed estuaries.

15 # 1 Introduction

Estuaries are tidal basins with some freshwater inflow, that are long relative to their inlet width. Reversing tidal flow is driven by the tidal water level fluctuations at the seaward boundary. In nature, estuaries have embayed or seaward widening planforms with coastal inlets and are partly filled with intricate patterns of shoals, tidal sand bars, mud flats and tidal marshes. The large-scale planform shape and bar-channel patterns within evolved by biogeomorphological processes and are partly determined by

20 inherited initial conditions and changing boundary conditions (de Haas et al., 2017). Certain phenomena are unique to estuaries, such as mutually evasive ebb- or flood-dominated channels separated by shoals (van Veen, 1950; Leuven et al., 2016). These shoals hinder shipping and at the same time may be important habitats. However, gaining understanding of their behaviour

is challenging because modelling sediment transport processes in three-dimensional reversing flow remains overly sensitive
to sediment transport parameters (van der Wegen and Roelvink, 2012), and field observations of morphological development
spanning decades to centuries are unavailable (Wang et al., 2002; Swinkels et al., 2009). The third, complementary method of
research is controlled laboratory experiments (Kleinhans et al., 2010), which are rare for estuarine phenomena in contrast to
5 the large number of river experiments.

 Only two sets of experiments simulating estuarine morphodynamics are accessible in the literature: Reynolds (1887, 1889)
conducted a large number of experiments in basins of various shapes, and Tambroni et al. (2005) conducted two experiments
in an exponentially widening estuary. In both cases the flow was driven by periodic sealevel fluctuations but sediment mobility
was too low compared to natural systems. Recently, an alternative experimental method was discovered (Kleinhans et al., 2012,
10 2014b, 2015) that caused sufficiently strong reversing flow for sediment transport similarity in tidal inlets by tilting the entire
flume periodically. With relatively small setups this was shown to result in dynamic channel and shoal patterns that are similar
to those in tidal inlet systems in nature. However, the experimental tilting principle was not yet applied to estuaries that are
much longer than tidal inlets and have more complicated tidal behaviour. Gentle tilting drives the flow in a fundamentally
different way than tides do in nature, raising the question to what degree this method leads to similar spatial flow and sediment
15 motion patterns. This paper presents a direct comparison of flow driven by periodic sealevel fluctuation and by periodic tilting
with the purpose of obtaining mobile sediment in laboratory settings.

 Tidal flows in natural estuaries can be complex but for the purpose of pioneering laboratory experiments only the funda-
mental properties are needed. Flow is mostly driven by a primary tidal component causing periodic sealevel fluctuation, which
propagates as a wave through the estuary mouth. This is modified by other tidal components, river flow and by circulation in
20 deep estuaries with salinity stratification (Dronkers, 1986; Friedrichs and Aubrey, 1988; Savenije, 2015). The length of an estu-
ary is typically up to half a tidal wavelength, which is estimated as $T\sqrt{gh}$ with primary tidal period T and shallow water wave
celerity $\sqrt{gh}$ where h is water depth. The tidal amplitude is usually less than half the water depth (Savenije, 2015). The result-
ing flow velocity depends on tidal period and inlet cross-sectional area, and on the tidal prism that depends on the planform
geometry of the estuary (e.g. Townend, 2012). Typically estuaries get narrower and shallower in landward direction as freely
25 erodible substrates adapt to spatial gradients in flow velocity, so that flow velocity in many estuaries does not vary more than an
order of magnitude with distance from the inlet (Savenije, 2015). The aerial extent and elevation of channels, shoals, mud flats
and saltmarshes modifies the magnitude, timing and duration of the ebb-directed flow and the flood-directed flow, particularly
if these vary along the estuary and if the channels are dredged (Wang et al., 2002). In turn, sediment mobility and transport
are driven by the flow to cause morphological change. Here, mobility is expressed as the Shields number $\theta = \tau/g(\rho_s - \rho)D$,
30 where τ is the bed shear stress by the flow, $g =$9.8 m/s^2 is gravitational acceleration, ρ and ρ_s are the density of water and sedi-
ment, respectively, and D is a representative particle size of the bed sediment. The bed shear stress is calculated as $\tau = \rho f u|u|$
where u is depth-averaged flow velocity driven by the energy gradient, and f is a dimensionless bottom drag coefficient. The
characteristic timescale of large-scale morphological change is much larger than the tidal period (van der Wegen et al., 2008;
Lanzoni and Seminara, 2002). This has an important consequence for modelling and experimentation: the phase differences of

flow velocity as a function of distance from the mouth are not of first-order importance for the morphodynamics, as long as spatial variations in velocity, residual currents and the resulting sediment mobility are present.

The prime challenge for morphodynamic experiments is that the reversing flow should cause sufficient bed shear stress for periodically reversing sediment motion (Kleinhans et al., 2015). As the bed sediment calibre cannot be scaled with the same ratio as the dimensions of the system, the energy gradient of the laboratory system must be increased such that the mobility remains the same as in the prototype, and for medium sands this slope typically is 0.01 m/m accounting for both particle weight and the large bed roughness in experiments (Kleinhans et al., 2014a). This required energy slope for mobile sediment is well feasible in river experiments, but not in estuary experiments with periodic sealevel fluctuation for the following reasons (Fig. 1). Assuming an experimental tidal system with a depth of 2 cm, the tidal water level amplitude can be at most about 1 cm. Given a typical aspect ratio of the estuary mouth of $W/h > 100$, this means that the width of the experiment should be about 1 m. However, with a minimum slope of 0.01 m/m, the distance from the mouth with sufficient gradient to move sediment is also about 1 m given the maximum water surface amplitude. In laboratory-sized systems this creates a short tidal basin (Stefanon et al., 2010; Kleinhans et al., 2015) rather than the long estuary we aim for. This leads to a number of scale problems. The first is a problem with tidal period. For the 2 cm depth and 1 m basin length this leads to a required tidal period of about 4-9 s, which is very short. The second problem is that this wave causes very low flow velocities of $O(10^{-3})$ m/s, which is far below that required for sediment motion. When the tidal amplitude is enlarged, a new problem arises: the flow causes net export of sediment results on the seaward sloping bed so that the tidal system excavates until it is in static equilibrium as probably happened in a number of the experiments of Reynolds (1889). An expensive solution would be to make impractical experimental setups of the order of hundreds of meters long, which renders morphological time scales impractically long. The tilting flume principle can perhaps attain the required sediment mobility, but the fundamentally different driving mechanism for the flow raises the question to what degree the tidal flow is similar to that in nature.

Therefore, measurements are needed of flow velocity fields and flow depth for a more in-depth analysis of the flow behavior compared to natural tidal systems, and a larger facility with a higher tilting frequency is needed for better scaling of basin size relative to tidal wavelength. The objective of this paper is to determine whether the tilting flume, in comparison with the Reynolds method, leads to reversing flow velocity and sediment mobility along the estuary similar to those in natural estuaries. To this end we present flow measurements in a new tilting flume facility and calculations with a one-dimensional model of the shallow water equations that has been adapted to include bed tilting. Specifically, experiments were designed to directly compare tidal wave behaviour, flow velocity magnitude and tidal asymmetry driven by periodic tilting or sealevel fluctuation in idealised straight tidal channels with rough beds and the largest possible tidal amplitudes. To exclude complex morphodynamic feedbacks, this study is limited to idealised channels without bars and shoals and with fixed rough beds or conditions below the beginning of sediment motion. Numerical tidal flow modelling was conducted at the same scale as the experiments. First the setup of the facility and measurement methods are outlined and the model is described, followed by results of the experiments compared to model results and discussion in the context of basic tidal flow patterns in idealised models of estuaries.

2   Design of the Metronome Facility

Between 2014–2015 we constructed the Metronome, a 20 m long flume designed for periodic tilting to create tidal systems (http://www.uu.nl/metronome, Fig. 2). For the purposes of future reference for ongoing biomorphological experiments and for replication in other laboratories the design of the Metronome is briefly described. The basic components are a steel basin that

5   tilts over the short central axis, motion control, water recirculation, and optical imaging (Fig. 3).

The steel basin has inner dimensions of 20.00 m long by 3.00 m wide and 0.40 m deep. The flume has two end tanks for water supply, water level control and outflow and for sediment trapping. The tilting axis is directly below the steel floor to minimise longitudinal motion and the entire flume setup is symmetrical about this axis. The basin was constructed from 4 mm stainless steel plates cut and folded such that the sidewalls are suitable for a gantry to screed the bed and set up measurement equipment,

10   and are a structural part of the basin to minimise bending. Further stiffness was accomplished by a ribbed structure and steel beams along and across the flume. Finite element modelling on the design showed that the maximum expected bending of the flume was 2 mm under extreme loads in emergency conditions, larger than expected in typical experiments. This model was also used to select the required range and power of the actuators and motion control and to estimate the loading and required reinforcement of the floor. The steel basin was curved slightly upwards during production such that it is straight under typical

15   water and sediment loading when supported by the tilting axis.

The end tanks were designed to function as constant head tanks, with sediment traps at the inside of a movable weirs. Water is supplied by four garden pond pumps with a maximum discharge of 4.7 L/s or 9 m head each in a 12 m^3 sump tank, which is an inflatable swimming pool in the basement of the building. The 3 m wide weirs in both end tanks are broad-crested with a length of 0.06 m and rounded edges due to the folding of the steel plate from which it was constructed. Small actuators control

20   the motion of the weirs. This setup means that the flow is critical on the broad-crested weirs, so that the water depth h_c at the weir depends on the specific discharge q over it as $h_c = \left(q^2/g\right)^{1/3}$. Consequently, the water surface elevation at the seaward boundary is not exactly as set by the weir height but is modified slightly depending on the tidal prism. The effect of this will be taken into account in the interpretation of the results herein. In future live-bed experiments the water depth can be corrected by motion of the weir at an appropriate amplitude and phaseshift relative to the tilting motion depending on the tidal prism.

25   The actuators to tilt the flume operate in pairs with motion mirrored at the tilting axis. The maximum force is 20 kN, but in downward direction had to be limited as reinforced concrete floor supports the downward force well but the upward, pulling force, not very well. The motion and forces are monitored and internal safety controls prevent values above this that might be damaging. The motion at periods and amplitudes as used in this paper is typically 0.01 mm accurate. The actuators keep repeatable positions at all times, also during rest, such that the flume does not deform. We found that the flume was best set

30   horizontal through manual measurement with a leveller and 0.5 mm graded rulers on the sand screed riding on the cart, and applying offset positions to all four tilting actuators.

Landscape experiments often show channels clinging to sidewalls, and, when insufficient sand is used, channels that erode down to the flume floor where erosion is enhanced because of the smooth surface. Using groynes or ribs are not solving this because these force their own patterns on the flow and morphology. We therefore covered the Metronome floor and sidewalls

with small-scale uniform roughness: an artificial grass of about 15 mm high, glued to the floor in places and kept down by a few mm of sand. The glue was applied such that water cannot flow under the grass. We used this roughness in the fixed-bed experiments and buried it under sand in the sand-bed experiments. The sand has a D_{10} of 0.33 mm, a D_{50} of 0.57 mm and a D_{90} of 1.2 mm.

3 Experimental Setup and Materials

3.1 Geometry and flow conditions

We conducted experiments with various initial and boundary conditions (Table 1). Most importantly, we applied periodic tilting and periodic sealevel fluctuation for comparison. Both experimental approaches were conducted on a sand-bed and on a rough, artificial grass bed. The majority of experiments were conducted on the artificial grass bed because this allowed most freedom in conditions that would have led to significant sediment motion on the sand bed. We tested two different boundary conditions for the tilting experiments with grass bed: one open sea boundary and one reflective boundary to represent an estuary with the landward boundary closed, and two open boundaries to represent a reach within a long estuary. We conducted auxiliary experiments with a constant flume gradient to test the flow resistance formulation for the artificial grass bed. The sand-bed experiments were conducted to assess effects of the typical roughness in live-bed experiments on the flow and had one open boundary in all cases. The sand-bed was pre-soaked.

The precise geometry of an estuary strongly determines tidal flow patterns along the river. Given the aim in this paper, we chose the simplest geometries and boundary conditions possible: straight channels and periodic motion (Table 1). For the artificial grass bed experiments, a straight channel of 0.7 m wide was sectioned off from the remainder of the flume by 0.1 m diameter cotton hoses filled with sand pressed down into the grass. For the sand bed experiments, a channel of 0.6 m wide and 0.03 m deep was carved in a 0.065 m thick sand-bed over the first 18 m of the flume, leaving a basin of 2 m long and 3 m wide uncovered. This 'sea' allows ebb delta formation in future live-bed experiments. The side effect is that the mass of water available for inflow and outflow of the channel is unhindered by the limited capacity of the pumps and the critical flow condition on the weir, making this setup insensitive to seaward boundary effects.

The average water depths were set at about $h =$0.028 m in all grass experiments by applying the same (average) heights of the weirs to submerge the vegetation-like roughness at all times. The Reynolds-type experiments were done with a period of 30 s and a seawater surface amplitude of 0.02 m, that is, the same period as in many of our other experiments and an extreme tidal amplitude, and a less energetic condition with a 60 s period and a 0.01 m amplitude that is closer to conditions in experiments reported in literature. The most basic tilting experiment has two open boundaries with constant elevations of both overflow weirs, approximating constant head conditions. For this condition two experiments were run with tilting periods of 30 s, which is similar to other experiments in literature, and 15 s to investigate the possibility of reducing the tidal excursion length. In most grass-bed experiments a tilting slope amplitude (maximum slope during sinusoidal tilting) of 9.1×10^{-2} m/m was applied. The second setup has one boundary closed (here at 0 m) and the other open, representing a tidal basin of finite

length. Here again 15 and 30 s periods were applied. As a control experiment to test the friction relation, the steady flow was measured at constant slopes of 0.91×10^{-3} m/m and 2.3×10^{-3} m/m and the same water depth as the other experiments.

Conditions in the sand-bed experiment were set such that the channel did not overflow and the sediment hardly moved, which was attained at a mean water depth of $h = 0.018$ m and a 40 s period, the typical period for live-bed experiments. The

5 Reynolds experiment on sand was conducted with 3.5×10^{-3} m water surface amplitude to prevent sediment motion. The tilting experiment was conducted with a tilting slope amplitude of 3.6×10^{-2} m/m, for which we observed no significant sediment motion.

3.2 Imaging, measurements and data reduction

Flow was measured by Particle Imaging Velocimetry (PIV) and manual water depth measurements. The PIV was conducted

10 by spreading white floating particles on the water surface of the flume, repeated photography and image processing to obtain the motion of the particles as detailed below.

Water depth was measured in the grass-bed experiments at various locations along the flume with rulers with 0.5 mm grading supported by small thin-legged tripods. This is rather inaccurate because of irregularities in bed elevation and because the meniscus of the water surface on the rulers. These data were detrended with still water measurements. In the sand-bed

15 experiments conducted later we measured water surface elevation relative to still water with an ultrasonic device at a sound frequency 150 kHz mounted on the tilting flume. The distance of about 0.2 m from the bed with temperature-corrected distance measurement resulted in a footprint of about 0.03 m and a vertical accuracy of about 1 mm. Measurements were collected for three tidal cycles at 10 Hz sampling frequency in phase with the tilting and phase-averaged by fitting with a spline at 1 s interval for presentation.

20 Seven industrial cameras were mounted 3.7 m above the floor of the flume, approximately above the centerline at equal distances. However, camera alignment was hampered by the roof supports in the temporary lab location so that axis positions and directions differ between cameras and are not perpendicular to the flume floor. This caused the geometry of the optical system relative to the flume to be suboptimal, resulting for higher tilt angles in a few pixels mismatch between adjacent cameras. This does not affect the conclusions of this paper because the velocity is spatially averaged along the flume and the focus is on

25 general characteristics and behaviour. The cameras are CMOS MAKO color cameras with a resolution of 2048 by 2048 pixels. The cameras have a lens with fixed focal length of 12.5 mm. The footprint is about 3.15 m, so that a pixel on average covers about 1.5–2 mm. Hardware and software are designed to allow simultaneous 25 Hz imaging for the purpose of PIV. The trigger for the cameras is taken from the tilting motor controller at exactly defined moments in the tidal cycle. For the PIV this trigger starts a 25 Hz pulse train from a frequency generator in order to have accurate, computer clock-independent timing.

30 The flume is illuminated at about 600 lux with daylight-coloured TL aimed at a white diffusive ceiling at about 4.5 m above the flume floor. This allows for low exposure durations, but we later found that the ceiling reflected on the water surface to hinder imaging in live-bed experiments. By the time we conducted the additional sand-bed experiments a diffusive white sheet was suspended below the ceiling and lamps in the shape of a tent. This improved lighting although it reduced light intensity, but this did not affect the PIV imaging.

The procedure for data collection was as follows. White floating particles of 2–3 mm diameter were seeded on the water surface along the flume, and newly supplied at both boundaries where necessary. After about five tidal cycles the flow was considered in equilibrium. In 16 phases of the tide, ten images were collected at 25 Hz simultaneously by all cameras. Water levels were measured before seeding the PIV particles. Control experiments with constant slope were conducted in the same

5   manner but with lower slopes because of the rapid evacuation of floating particles.

Images were first debayered to obtain RGB color images, from which only the green layer was taken for analysis. Background images were subtracted that were obtained for the same tidal phase without floating particles. These images were then rectified using the Caltech camera calibration toolbox in Matlab (http://www.vision.caltech.edu/bouguetj/calib_doc/, version October 15, 2004), after obtaining camera calibrations.

10   Flow velocities were calculated for every pair of consecutive images using the MPIV toolbox in Matlab (by Nobuhito Mori, 2009). The focus of this paper is on width-averaged flow in a uniform channel, so that the conventional cross-correlation algorithm for PIV suffices. This means that the peak cross-correlation is used as mean particle displacement in a given window. This was run with a window size of 100 pixels with 50% overlap. Subsequently the vector fields were scaled by the footprint of the cameras which was calculated from the geometry of the flume, average height of cameras and camera resolution and the

15   instantaneous tilting angle. Erroneous vectors resulted from windows that were partially filled with flume wall, spots empty of particles, mismatched particles and reflections on the water surface. After filtering out the 1% most extreme values, width-averaged velocities were obtained along the flume for each cross-section.

4   Numerical Flow Model

4.1   Model formulation

20   Here present a one-dimensional model modified to tilt the bed periodically. The scenarios of initial conditions and boundary conditions are the same as in the experiments.

Continuity is conserved as:

$$w\frac{\partial h}{\partial t} = \frac{\partial uwh}{\partial x} \tag{1}$$

where w =width, h =depth and the product of these is the cross-sectional area A in our rectangular channel, u =flow velocity,

25   water depth $h = \eta + z_b$, with water surface located at level $z = \eta$, bed bed level at $z = -z_b$, t =time and x =streamwise coordinate. The left-hand side represents the time rate of change of the wetted cross-sectional area and the right-hand side represents volume flux convergence along the channel. Note that by tilting the basin z_b is a function of time. This means that water depth can change because both bed-level and water surface are function of time and space.

The momentum balance equation is given as:

30   $$\frac{\partial Q}{\partial t} + gA\frac{\partial \eta}{\partial x} + g\frac{Q|Q|P}{C^2A^2} = 0 \tag{2}$$

where the terms from left to right represent local acceleration, along-channel pressure gradient and bottom friction. Further, $C =$Chezy roughness coefficient and $P =$ is the wetted perimeter.

The model is discretized on a staggered grid with n flux points and $n-1$ bed elevation points and applies an explicit numerical scheme that is second order in both time and space. The condition that Courant numbers for surface wave celerity and flow velocity are below unity was checked for every model run. Typical model settings are a time step of 0.05 s and a spatial step of 0.05 m.

4.2 Hydraulic resistance

The artificial grass cover of the Metronome floor causes hydraulic resistance similar to that of submerged unbending vegetation. This flow resistance is calculated with the relation found by Baptist et al. (2006, their Eq. 74). Furthermore, the surface flow velocity is derived from the model calculations in order to be able to compare with the PIV data.

The Chezy roughness coefficient for submerged vegetation is calculated as the combined effect of bottom roughness, through-flow resistance and overflow resistance (Fig. 4a):

$$C = \sqrt{\left(\frac{1}{C_b^2} + \frac{c_D n_s D_s H_s}{2g} \right)^{-1}} + \frac{\sqrt{g}}{\kappa} \ln \frac{h}{H_s} \qquad (3)$$

where $n_s =$number of stems, here measured at 50,000 m^{-2}, $D_s =$stem diameter, here measured at 0.4 mm, $H_s =$vegetation height, here 14 mm, and $\kappa =$Karman's constant (0.4). The first term represents the bed friction below the vegetation; the second term represents the flow through the vegetation and the third term represents flow over the vegetation. The drag coefficient c_D of vegetation is here taken dependently on the Reynolds number $Re = uh/\nu$ with $\nu = 1 \times 10^{-6}$, because during flow reversal it may well drop below typical turbulent flow values. The drag coefficient is dynamically calculated with the Coleman constitutive relation:

$$c_D = 1 + \frac{30}{Re} + \frac{15}{Re^{0.6}} \qquad (4)$$

so that for high Re, $c_D \approx 1$. We assume a minimum $Re = 30$ so that the maximum $c_D \approx 4$, which occurs for velocities below about 0.001 m/s. The roughness of the bottom of the vegetated layer is calculated as:

$$C_b = 18_{10} \log \frac{12h}{k_s} \qquad (5)$$

where $k_s =$is the Nikuradse roughness length, here taken to be equal to the 90th percentile of the particle size distribution at 1.23 mm, where the median is 0.56 mm. In the sand-bed experiments a constant $C = 25$ m$^{0.5}$/s was assumed. The dimensionless friction factor is calculated from the Chezy coefficient as:

$$f = \frac{g}{C^2} \qquad (6)$$

To be of use for the present purpose, the flow velocity at the water surface is needed for comparison of model results with PIV-derived data. Corrections usually reported in literature assume a logarithmic flow velocity profile, but in the present case

a layer of water is 'skimming' over the vegetation so that the partitioning of flow between lower and higher layers differs. A correction factor was therefore analytically calculated by combination of equations in Baptist et al. (2006) for a range of water depths above the submergence height of the vegetation. The ratio of surface velocity and depth-averaged velocity was found to be insensitive to total water depth (Fig. 4b), meaning that water depth variations during the tidal cycle do not change the

5 ratio between depth-averaged and surface velocity more than, say, 5–10%. Here flows with emergent vegetation are ignored because the present method of PIV is impossible to use under these conditions. Furthermore, the flow is not well described for the transition between barely submerged vegetation to emerged vegetation where the aforementioned ratio rapidly drops to unity, so these conditions are avoided. In the remainder of this paper the modelled velocities are corrected with a constant multiplication factor of 1.95 for the grass-bed experiments and 1.60 for the sand-bed experiments, which leads to an error of at

10 most ±5% for the lowest and highest water levels, respectively.

5   Results

Comparison of all experiments shows that flow velocities in the tilting flume are much larger than in the Reynolds setup. High velocities occur nearly simultaneous along the flume as expected because it is driven by the gradient of the entire flume rather than the gradient caused by a tidal wave initiated at the seaward boundary. These results are consistent with the numerical

15 model. Below the results are described in detail.

5.1   Tilting flume experiments with two open boundaries

The tilting with two open boundaries shows nearly symmetrical reversing flow (Figs 5,6). Spatial patterns in flow velocity along the flume appear consistent between tidal phases and with the unidirectional flow experiments and are caused by camera alignment and irregularities on the flume bed. These are further ignored. The flow velocity lags behind the periodic tilting with

20 about 2-3 seconds in both the 30 s and 15 s period tilting (Fig. 5b and Fig. 6b). Measured water level fluctuates periodically near the boundaries, especially at the 20 m boundary (Fig. 5c). The faster tilting (15 s) experiment has a lower velocity amplitude that also occurs nearly simultaneous along the flume. On the other hand the slower tilting has a higher velocity amplitude in the middle of the flume. The slower tilting also shows more deformation in the velocity signal than the faster tilting (compare Fig. 5b and Fig. 6b).

25   The model results show a fairly simple periodic flow that is nearly uniform along the flume, with a very minor reduction of flow velocity at the boundaries (Fig. 5a). Likewise, the modelled water levels are nearly static (Fig. 5c). Modelled flow velocities fit the observations fairly well when local accelerations due to bed irregularity and discontinuities due to camera positioning are ignored. However, a wave forms at both boundaries in all tilting experiments that lead to velocity peaks coinciding with water level peaks.

30   The time lag differs between the model and the flume (Fig. 5b), so that the highest velocities of the tidal cycle are approximately modelled correctly but there is a mismatch between model and observations near the slack. The measured flows begin to decelerate sooner after the peak and accelerate slower after the slack, while the modelled flow has a more rapid reversal of

flow. A possible reason is that the water depth varies with about 5 mm in the experiments over the tidal cycle, which changes inertia, whereas the modelled water depths show no significant temporal variation. In the flume there are stilling basins from which water flows in at nearly zero velocity to rapidly accelerate into the flume. In the model, on the other hand, there is no velocity gradient at the boundaries. An additional explanation is the effect of the critical flow over the weir and the capacity

5 of the pumps. During inflow, the water depth at and near the boundary reduces as the pump capacity is constant because less water flows out of the flume. This reduces the inflow velocity. This effect could in future be removed by increasing the pump capacity or decreasing the effective width of the channel. During outflow, the water depth at and near the boundary increases as the broad-crested weir forces flow to be critical. This effect could in future be removed by compensation of the weir elevation.

We compared the amplitudes and phases of tidal components in the observed and modelled velocity signals in the middle of

10 the flume (Fig. 7). For clarity the full tilting period of the flume is called 'principal tide' or 'T1' rather than M2. The comparison shows that the tidal velocity signal is dominated by the tilting period. The 'second overtide' (T3 rather than M6) is about 2% of the velocity amplitude due to friction and the 'first overtide' (T2 rather than M4) is even lower due to the negligible water level fluctuations. For the latter the deviation between modelled and observed velocity is also the largest but this cannot be considered significant given an uncertainty in the velocity data of a few percent. This is another representation of the difference

15 in acceleration and deceleration or insufficient pump capacity noted before. The phase lag of T3 surprisingly is opposite in the model compared to the observations. However, the phase lags are much smaller for the principal tide.

5.2 Tilting flume experiments with one open boundary

The observed and modelled flows in experiments with one boundary closed are fairly similar to those with two open boundaries with two major differences (Figs 8,9). First, the flow velocity reduces to zero at the closed boundary over a distance of about

20 1–2 m for the flood current (towards the closed boundary) in both experiments, and increases to its maximum value over a distance of about 5 m for the ebb current in the 30 s experiment and about 3 m in the 15 s experiment. This asymmetry between ebb and flood currents is caused by the fact that water depth increases during the flood stage and decreases during the ebb stage.

The second difference with the open boundary experiments is the effect of reflection of the tidal wave on the closed boundary.

25 This leads to water depth and velocity fluctuations close to the boundary (Fig. 8). As a result a water surface wave with a velocity peak travels seaward over an 8–10 m distance whilst the tilting slope peaks and reverses, to dampen out at the peak flood velocity. The primary effect of this wave superimposed on the tilting is a reduction of velocity near the upstream boundary. In the middle and downstream reaches of the flume, the observed and modelled flow shows negligible differences with the cases of two open boundaries. We visually observed that the wave formed a bore of several millimeters high in the

30 experiments.

The modelled and observed water level amplitudes at the upstream boundary agree fairly well (Fig. 8c). The absolute level differs, but this is meaningless in the experiments because the data was detrended.

The harmonic analyses show that the runs with one boundary closed plot close to the runs with both boundaries open for all tidal components, except for the T2 that is two orders of magnitude smaller than the T1 (Fig. 7). This means that the flow in the middle of the flume is not affected by the upstream boundary being closed, in agreement with the observations made above.

5.3 Reynolds-type experiments

5 Flow in the Reynolds setup with periodic sealevel fluctuations is weak (Figs 10). The 30 s experiment with the amplitude exceeding half a water depth showed effects of drying and flooding, invalidating this experiment for the present purposes. In general the strongest flows are generated at the sealevel boundary, decaying rapidly towards the closed boundary. The data show that velocity halves within the first 3 m in both experiments. Furthermore, a local minimum velocity occurs in the middle of the flume and a slight increase in flow velocity at one quarter of the length with opposite phase to that at the mouth. The
10 numerical model roughly reproduces this pattern but predicts higher velocities in the upstream half of the flume than observed.

However, this experiment shows a velocity limitation. Even though a 0.01 m sealevel amplitude was imposed, the observed sealevel amplitude at 0.1 m from the upstream boundary is only half this value. This may be due to the pump capacity limitation at the seaward boundary. For this reason we ran the model with half the design amplitude, which resulted in fairly close correspondence of flow velocity in the most seaward few meters. Furthermore, higher modelled water level amplitudes did not
15 result in equally higher flow velocities because of the nonlinear effects of friction in shallower flow.

5.4 Sand-bed experiments

The sand-bed experiments with the tilting and Reynolds setups behave largely the same as the grass-bed experiments (Figs 11,12). The flow velocity amplitude is much larger in the tilting experiment than in the Reynolds experiment, despite the modest tilting slope amplitude. Despite the perfectly symmetrical tilting motion, the ebb and flood phases are asymmetrical: flood velocities
20 occur at higher water levels than the same ebb velocities in the first few meters from the closed boundary despite the perfectly symmetrical tilting motion. On the other hand, the velocity amplitude in the Reynolds experiment decays rapidly in landward direction, but the sealevel amplitude is already 30–40% of the water depth and cannot sbe increased much.

The sand-bed experiments have a complex geometry with a narrow, shallow channel connected to a wide and deep sea. This leads to two-dimensionality in the flow pattern that the one-dimensional model cannot cover well, such as the high peak
25 in modelled flow velocity at the transition from sea to channel, which is more gentle in the experiment due to convergence and divergence in the sea. Also the large spread in the flow velocities at $x = 18.6$ m in Fig. 11b and Fig. 12b is due to the two-dimensional variation. The spatial and temporal patterns in the data are qualitatively similar to the model results with magnitudes of flow velocity within about 20%. However, despite the water available in the sea for rapid inflow and outflow of the channel, and the narrowed flume, the inflow velocity again appeared to be limited. This suggests that the pumps are not
30 limiting the inflow after all. We speculate that the inflow from the stilling basin (and sediment trap) over a sharp edge onto the grass-covered flume floor causes flow losses. When half the sealevel amplitude was imposed in the model, as in the grass-bed experiments, we obtained a velocity and water level amplitude similar to that in the experiments.

As in the grass-covered experiments, bores of a few millimeter high form. A small ebb bore intiates near the upstream boundary and a larger flood bore iniates at the seaward boundary. Furthermore, the measured velocity amplitude reduces faster in landward direction than the modelled velocity in the Reynolds experiments. This is surprising, because with a sea present in the tilting flume we do not expect the flux from the seaward boundary to be limited by the pumps so we did expect the

5   measured flow to resemble the model better.

The sand-bed experiments were designed as the initial condition for live-bed experiments to be done later and are in that sense closer to future morphological experiments than the grass-bed experiments. However, the sudden transition from sea to channel renders the data less straightforward to interpret. Nevertheless the general correspondence in behaviour between the grass-bed and sand-bed experiments and the model runs shows consistent behaviour of the tilting flume in comparison to the

10   Reynolds setup, which allows general conclusions.

5.5   Control experiments with constant slope

Measured flow in the constant slope experiments is on average uniform as expected (Fig. 14). However, there are spatial variations up to 20% that are consistent between the two experiments for flow velocity and for water depth. Some of the variation occurs at the transitions between camera images, which can be explained by deviations in camera orientation. However, a larger

15   part is also seen in the water depth measurements including the still water depth and can therefore be attributed to irregularities in the elevation of the artificial grass and the thickness of the sand bed. For example, the increased velocity at 16–18 m coincides with shallower flow and the lowest velocities occur at 6–7 m and 12–13 m.

The highest water depths occur at the upstream boundary (0 m) and the downstream boundary (20 m), perhaps because here the grass was glued to the flume floor and the sand was not spread out as well. Water depth is lowest for the highest flow

20   velocity as expected because only slope was changed. The effect of this will be tested with the numerical model later.

The predicted flow velocity based on measured average water depth and imposed slope is about correct, which we take as sufficient evidence that the measured artificial vegetation characteristics lead to the correct predicted friction coefficient in the model. The effective Chezy coefficient is about 11 $\sqrt{m}/s$ for these conditions, which is typical for shallow flume experiments with rough bed.

25   ## 5.6   Numerical exploration of typical tilting flume conditions

We use the model to explore behaviour of a tilting system over a larger parameter space than accomplished in the experiments. First we analyse tidal asymmetry and magnitudes of overtides, followed by a test run with depth variation along the flume to assess to what degree grass and sand bed irregularities in the flume affected the tidal flows.

Tidal asymmetry is often used to indicate sedimentation tendencies. This was here calculated as a function of the tilting

30   slope amplitude. The ratio of peak flood and peak ebb flow velocity (Fig. 15a) indicates whether tidal basins are respectively importing or exporting sand. The ratio of flood and ebb duration between the peak flows (Fig. 15b), on the other hand, indicates the tendency for mud sedimentation at slack tide. Here, flood duration is defined as the period between peak ebb to peak flood velocity and the ebb duration as the period between peak flood to peak ebb velocity.

The closed landward boundary has higher flood velocities and longer ebb duration (Fig. 15), meaning that the head of the estuary fills rapidly and empties slowly. This would lead to sedimentation as expected with principal tide and without river inflow. The inlet has approximately symmetrical tides but is slightly ebb-dominant. Halfway the flume and in upstream direction the currents are ebb-dominated and the ebb duration is also longer than the flood, which was found earlier to be

5 mostly due to a minor second overtide contribution. The behaviour towards and at the upstream boundary is sensitive to the tilting amplitude: above the large gradient of 0.02 the currents become flood-dominant and the flood duration exceeds the ebb duration. Note, however, that the strongest responses all occur in the upstream few meters of the flume, where, in a live-bed experiment, sedimentation would rapidly modify the morphology, which would reduce these asymmetries.

The sensitivity of the flow to water depth variations is rather large (Fig. 16): a gradually increased depth with a maximum of

10 5 mm, less than 20% of the original depth, already causes large spatial variations in flow velocity and depth. In particular, the increased depth causes increased ebb velocities at the seaward boundary during some phases, and decreased flood velocities. The flow velocity patterns with modified bed elevation are more nonuniform even in the middle of the flume (Fig. 16a) and resemble those observed in the experiments. This makes it likely that the irregularities of the bed in the experiments caused at least some of the deviations between the model and experimental data, in addition to potential bias in the data due to imperfect

15 camera positioning and calibration. This does not affect our main conclusions in view of future live-bed experiments, however, because the aforementioned bed elevations were imposed. It is expected that self-formed morphology will not cause such strong spatial variations in flow velocity, because these would cause spatial gradients in sediment transport that modify the morphology to reduce eventually the spatial variations in flow velocity.

Two main differences emerged between the model and the data (Fig. 16 and Fig. 13) that need to be taken into account in

20 interpretations. Firstly, the water level amplitude is smaller in the experiments than in the model while flow velocity amplitude is larger in the experiments. Secondly, bores form in the experiments during both flood and ebb phases. In both model and experiments the tidal flow at the sealevel boundary transitions from currents without water level fluctuations, to water level fluctuations without current fluctuations at the closed landward boundary.

6 Discussion

25 The key result of the experiments and numerical modelling is that the periodic flow velocities in a tilting flume setup are roughly uniform along the tilting flume. In contrast, periodic fluctuation of the sealevel as in Reynolds setup causes much lower velocities that decay rapidly in the landward direction. Here we discuss several basic considerations for scaling between the types of experiments and full-scale estuaries in nature.

The effect on sediment transport would be that sediment is immobile along most of the Reynolds setup and mobile in the

30 tilting setup (Fig. 17). Here the grain-related Shields number is calculated from the depth-averaged flow velocity and skin-friction as $\theta = \rho u^2 / [C_b^2 (\rho_s - \rho) D]$ for the sediment used as bottom layer in the artificial grass. The ongoing morphological experiments (Fig. 2) are also conducted with this sediment. Peak values of the Shields number in the tilting experiments with grass bed are 0.2–0.3. In the sand-bed experiments, with lower tilting slope amplitude, mobility was kept deliberately at about

the threshold for motion, but much larger values can be obtained by higher tilting slopes. This means that the typical mobilities of natural systems, which are of the order of 0.5–1, are within reach with the Metronome, which is one of the most important variables to scale in landscape experiments (Kleinhans et al., 2014a).

The experimental water depths mean that the tidal wave celerity is expected to be about 0.52 m/s in the grass-bed experiment and 0.42 m/s in the sand-bed experiment. With depth-averaged velocities being considerably smaller the Froude number in the experiments is well below unity. Given the length of 20 m of the flume, this tidal wave celerity means that basin length normalised by tidal wavelength is 1.27 for the 30 s period 2.54 for the 15 s period experiments with grass bed. For the sand-bed of 18 m length and 40 s period this ratio is 0.93. In reality tidal basins have lengths of one quarter to half a tidal wavelength, so that the flume represents a long tidal basin in the situation with one open boundary. Furthermore, with two open boundaries the flume simulates a limited reach in an estuary with a nearly static water surface and periodic flow velocity, that is similar to the rigid lid assumption in tidal bar theories (Leuven et al., 2016).

The tidal excursion length, i.e. the path that a parcel of water travels during half a tidal cycle, is another measure indicative of the scaling of the experiments in addition to the sediment mobility and the length relative to tidal wavelength calculated in the methods section. In a natural estuary with a velocity amplitude of 1 m/s (Savenije, 2015) and tidal period 12.4 hr, the tidal excursion length is of the order of 20 km, while an intermediate-sized estuary of 10 m deep has a tidal wavelength of 400 km, so that its length is of the order of 100 km which is five times the tidal excursion length. In the experiments the tidal excursion length is 3–4 m while the aforementioned wavelength is about five times larger as in the natural case. Furthermore the ratio of tidal water level amplitude and water depth is about 0.2–0.4 in the experiments, which is also fairly similar to that in nature.

The broad similarity between conditions in the 15, 30, 40 and 60 s conditions shows that a range of combinations of tidal wavelengths, tidal excursion lengths and sediment mobility can be attained in the Metronome to design preferred scales. Furthermore it is technically straightforward to tilt the Metronome with higher harmonics and tidal asymmetry, to add a constant discharge at one closed boundary, and to impose any initial planform shape and depth along the system. This means that it is possible to drive ebb- or flood-dominant transport in the flume, which is the cause of sediment import, export and equilibrium in natural systems (Dronkers, 1986; Wang et al., 2002; Schuttelaars and de Swart, 2000). Moreover, a mobile bed may develop to form any equilibrium estuary under given boundary conditions without imposing an initial shape or depth, which is the aim of ongoing experiments.

However, the principle of the tilting flume is counterintuitive: the real world does not tilt periodically. This may be the reason that this principle was not invented in the past 130 years. Whilst a comparison of tidal wave and flow properties in the experiments and full-scale systems is not straightforward, the comparison with the numerical model shows that the flow behaves as expected when the physical processes are included that are commonly used in estuarine flow models (Friedrichs and Aubrey, 1988; Li and O'Donnell, 1997). We observed bores in all experiments that are possibly caused by the high slope (Dronkers, 1986) but of which the morphological effects remain to be studied. Furthermore the dominant tidal components are similar: data shows that shallow bar-built estuaries are commonly dominated by the M2 tide (Wang et al., 2002) in nature and the principal tide in the Metronome, with additional spring-neap tidal variations due to the S2 and M4 generated by friction in nature. Given estuaries with a state somewhere between a weakly ebb-dominated and weakly flood-dominated, the net sediment

transport patterns are strongly dependent on the relative areas of shoals and channels, on the generation of overtides and the presence of river influx. We are currently testing whether all these conditions can be generated in the tilting flume setup.

It is clear from the present results that obtaining sufficiently mobile sediment over the length of an experimental estuary is impossible in the Reynolds setup at practical laboratory sizes. On the other hand, it is possible with the Metronome. With this,

5 the question whether flooding or tilting is better suited for morphodynamic experiments of tidal systems is partially answered in that the tilting method is clearly more suited to obtain periodically reversing sediment transport at any required mobility similar to that in natural systems. This suggests that the Metronome setup opens up the possibility to conduct experiments on estuary development and biogeomorphodynamics following similar principles as for rivers, including interactions with self-forming floodplains of cohesive sediment and vegetation (Kleinhans et al., 2014a). Moreover, this technology is potentially

10 widely available because of the simplicity of periodic tilting and the small flume size at which interesting results are obtained (Kleinhans et al., 2015).

7   Conclusions

The method of Reynolds with periodically fluctuating sealevel cannot lead to sufficient bed shear stress for bidirectional sediment transport except in impractically much larger setups and with low-density sediments. The most important reason is

15 the limitation in tidal amplitude relative to water depth. Furthermore the tidal wave rapidly dampens out in landward direction due to friction, that is higher in experiments than in nature. Technically, these experiments require considerable pumping capacity even to reach the limited mobility in the inlet.

A periodically tilting flume causes reversing flows with sufficient strength in both flood and ebb direction to transport sand. A simple sinusoidal tilting pattern with two open boundaries causes an approximately sinusoidal flow velocity pattern along

20 the entire flume with uniform width and depth whilst water level hardly fluctuates, which means that the rigid lid condition is approximated with two open boundaries. When one boundary is closed, reflection of the tidal wave causes large depth fluctuations and enhanced ebb currents near the closed boundary, whilst the flow velocity along most of the flume is almost the same as in the experiments with two open boundaries. The flow velocity pattern is quite sensitive to water depth variations of the irregular rough flume floor, which indicates that there would be significant interaction between the flow and a mobile

25 sediment bed. The flow remains subcritical but the Froude number is much larger than in natural estuaries. In nature this would affect tidal wave propagation and resulting flow velocity, but in the tilting flume the tidal wave is independently imposed by the tilting, which allows independent control over flow magnitude and period. This, in turn, allows experimental control over the simulated length of the tidal basin and the tidal excursion length without compromising the sediment mobility.

Certain phenomena emerge in the tilting flume conditions of which the effects on morphological development remain to be

30 studied, such as a tidal bore and the reflection on the landward boundary when that is closed. On the other hand, the strong three-dimensional effects in the transition from the shallow sea to the inlet, complicating the comparison with the numerical model, may represent similar phenomena in nature well.

The tilting leads to two unexpected effects that need to be cancelled by periodic motion of the overflow weir. Flow depth over the weir is controlled by the specific discharge given that the Froude number remains constant. This means that compensation is required, approximately in phase with the tilting and depending on discharge to maintain constant sealevel. This suggests better experimental results further away from the boundary that could be attained by installing a 'sea' over a length of a few

5 meters. However, the tilting causes additional flow in the sea that leads to water level change at the coastline. This can be prevented by opposite-phase correction of the downstream weir to maintain constant sealevel at the coastline rather than at the weir.

The technical possibility to use a large tilting gradient allows a similar sediment mobility as in natural systems over relatively large distances away from the estuary mouth. The implication is that the Metronome tidal facility opens up new possibilities

10 for tidal morphodynamics research that are complementary to numerical modeling and field observations.

Author contributions. The authors contributed as follows: idea of flume tilting and principal investigator: MK, numerical model development: MV, numerical modelling: MK and MV, data collection: MK, JL and LB, data analyses: MK and JL, manuscript preparation: MK with contributions from JL, LB and MV. MvM and MK led the design and building project, HM and AS did the technical design of the Metronome, CR, HM and AE designed and built the pumping system, PV led laboratory infrastructure design and construction. Original

15 images and matlab image processing scripts are available upon request from the first author, as are technical drawings and other information about the Metronome.

Acknowledgements. Comments by reviewers and guidance by the editors will be gratefully acknowledged. The research by MK, JL and LB and the construction of the Metronome were funded as a Vici grant to MK by the Dutch Technology Foundation (STW) that is part of the Netherlands Organisation for Scientific Research (NWO, grant 016.140.316). We acknowledge collaboration with Variodrive, who designed

20 and programmed the actuators, Bart Boshuizen (TU-Delft) who programmed the motion, HiH engineering, who modelled the forces on the steel construction, and Stemmer Imaging, who designed and programmed the imaging system. Data and building plans of the Metronome and of a 3 m long steel mini-Metronome available from MK upon request.

References

Baptist, M., Babobic, V., Rodriguez Uthurburu, J., Keijzer, M., Uittenbogaard, R., Mynett, A., and Verwey, A.: On inducing equations for vegetation resistance, J. of Hydraulic Res., 45, 1–16, 2006.

de Haas, T., Pierik, H., van der Spek, A., Cohen, K., van Maanen, B., and Kleinhans, M.: Long-term evolution of tidal systems: effects of rivers, coastal boundary conditions, eco-engineering species, inherited relief and human interference, Earth-Science Reviews, 2017.

Dronkers, J.: Tidal asymmetry and estuarine morphology, Netherlands Journal of Sea Research, 20, 117–131, 1986.

Friedrichs, C. and Aubrey, D.: Non-linear tidal distortion in shallow well-mixed estuaries: a synthesis, Estuarine, Coastal and Shelf Science, 27, 521–545, 1988.

Kleinhans, M. G., van der Perk, M., and Bierkens, M.: On the use of laboratory experimentation: "Hydrologists, bring out shovels and garden hoses and hit the dirt", Hydrol. Earth Syst. Sci., 14, 369–382, 2010.

Kleinhans, M. G., van der Vegt, M., Terwisscha van Scheltinga, R., Baar, A., and Markies, H.: Turning the tide: experimental creation of tidal channel networks and ebb deltas, Netherlands J. of Geoscience, 91, 311–323, 2012.

Kleinhans, M. G., van Dijk, W., van de Lageweg, W., Hoyal, D., Markies, H., van Maarseveen, M., Roosendaal, C., van Weesep, W., van Breemen, D., Hoendervoogt, R., and Cheshier, N.: Quantifiable effectiveness of experimental scaling of river- and delta morphodynamics and stratigraphy, Earth-Science Reviews, 133, 43–61, doi:10.1016/j.earscirev.2014.03.001, 2014a.

Kleinhans, M. G., van Rosmalen, T., Roosendaal, C., and van der Vegt, M.: Turning the tide: mutually evasive ebb- and flood-dominant channels and bars in an experimental estuary, Advances in Geosciences, 39, 21–26, doi:10.5194/adgeo-39-21-2014, 2014b.

Kleinhans, M. G., Terwisscha van Scheltinga, R., van der Vegt, M., and Markies, H.: Turning the tide: growth and dynamics of a tidal basin and inlet in experiments, J. of Geophys. Res. Earth Surface, 120, 95–119, doi:10.1002/2014JF003127, 2015.

Lanzoni, S. and Seminara, G.: Long-term evolution and morphodynamic equilibrium of tidal channels, Journal of Geophyiscal Research C, 107, doi:10.1029/2000JC000468, 2002.

Leuven, J., Kleinhans, M. G., Weisscher, S., and van der Vegt, M.: Tidal sand bar dimensions and shapes in estuaries, Earth-Science Reviews, 161, 204–223, doi:10.1016/j.earscirev.2016.08.004, 2016.

Li, C. and O'Donnell, J.: Tidally driven recirculation in shallow estuaries with lateral depth variation, J. of Geophys. Res., 103, 27 915–27 929, 1997.

Reynolds, O.: On certain laws relating to the regime of rivers and estuaries and on the possibility of experiments on a small scale, Br. Assoc. Rep., London, 555–562, 1887.

Reynolds, O.: Report of the committee appointed to investigate the action of waves and currents on the beds and foreshores of estuaries by means of working models, British Association Report. In: Papers on mechanical and physical subjects, Vol. II 1881-1900, Cambridge Univ. Press, 1901, Chapter 57, 380-409, 1889.

Savenije, H.: Prediction in ungauged estuaries: an integrated theory, Water Resour. Res., 51, 2464–2476, doi:10.1002/2015WR016936, 2015.

Schuttelaars, H. M. and de Swart, H. E.: Multiple morphodynamic equilibria in tidal embayments, Journal of Geophysical Research C, 105, 24 105–24 118, 2000.

Stefanon, L., Carniello, L., D'Alpaos, A., and Lanzoni, S.: Experimental analysis of tidal network growth and development, Continental Shelf Research, 30, 950–962, doi:doi:10.1016/j.csr.2009.08.018, 2010.

Swinkels, C., Jeuken, C., Wang, Z., and Nicholls, R.: Presence of connecting channels in the Western Scheldt Estuary, J. of Coastal Research, 25, 627–640, doi:10.2112/06-0719.1, 2009.

Tambroni, N., Bolla Pittaluga, M., and Seminara, G.: Laboratory observations of the morphodynamic evolution of tidal channels and tidal inlets, J. Geophys. Res., 110, F04 009, 2005.

Townend, I.: The estimation of estuary dimensions using a simplified form model and the exogenous controls, Earth Surf. Process. Landforms, 37, 1573–1583, doi:10.1002/esp.3256, 2012.

5 van der Wegen, M. and Roelvink, J.: Reproduction of estuarine bathymetry by means of a process-based model: Western Scheldt case study, the Netherlands, Geomorphology, 179, 152 – 167, doi:10.1016/j.geomorph.2012.08.007, 2012.

van der Wegen, M., Wang, Z. B., Savenije, H. H. G., and Roelvink, J. A.: Long-term morphodynamic evolution and energy dissipation in a coastal plain, tidal embayment, Journal of Geophysical Research: Earth Surface, 113, F03 001, doi:10.1029/2007JF000898, http://dx.doi.org/10.1029/2007JF000898, 2008.

10 van Veen, J.: Ebb and flood channel systems in the Netherlands tidal waters, Journal of the Royal Dutch Geographical Society, 67, 303–325, 1950.

Wang, Z., Jeuken, M., Gerritsen, H., de Vriend, H., and Kornman, B.: Morphology and asymmetry of the vertical tide in the Westerschelde estuary, Continental Shelf Research, 22, 2599–2609, 2002.

Table 1. Boundary conditions applied in all experiments: auxiliary fixed-slope experiments to determine the roughness of the artificial grass bed, periodic tilting experiments with one or two open boundaries, and periodic sealevel variations. Experiments with sand bed were conducted with a shallow sea of 2 m length to reduce boundary effects and were closed on the upstream boundary.

bed	period	tilt slope amplitude	sealevel amplitude	boundaries	rationale
	s	$\times 10^{-3}$ m/m	$\times 10^{-3}$ m		
grass		0.9	0	both open	steady flow: control
grass		2.3	0	both open	same, faster flow
grass	60	0	10	x=0 m closed	same, longer wave
grass	30	0	20	x=0 m closed	Reynolds method
grass	30	9.1	0	both open	reach within estuary
grass	15	9.1	0	both open	same, shorter tidal excursion length
grass	30	4.5	0	both open	reduced tidal energy (not shown)
grass	30	9.1	0	x=0 m closed	basin with reflective landward boundary
grass	15	9.1	0	x=0 m closed	same, short tidal excursion length
sand	40	3.6	0	x=0 m closed	tilting, natural roughness
sand	40	0	3.5	x=0 m closed	Reynolds method, natural roughness
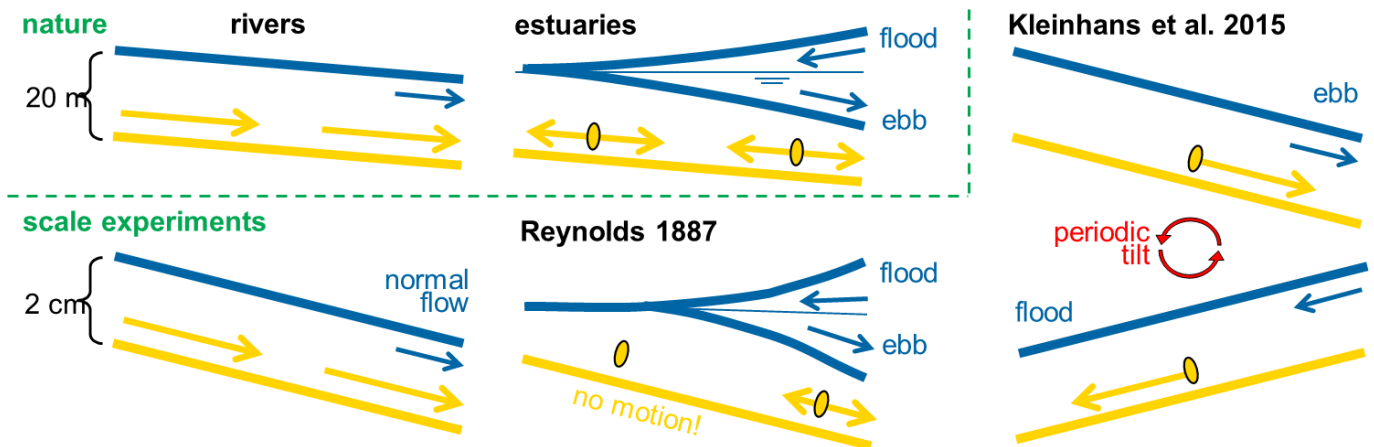
Figure 1. Driving flow in nature and in experiments with the requirement of sediment mobility similarity. Given the same sediments in experiments as in natural systems, the shear stress in experiments must be the same as in nature. With much smaller water depths this requires much larger gradients, which is straightforward for river experiments. In tidal experiments these gradients are impossible to obtain in flumes by sealevel fluctuation, but quite feasible to obtain by tilting the flume periodically.
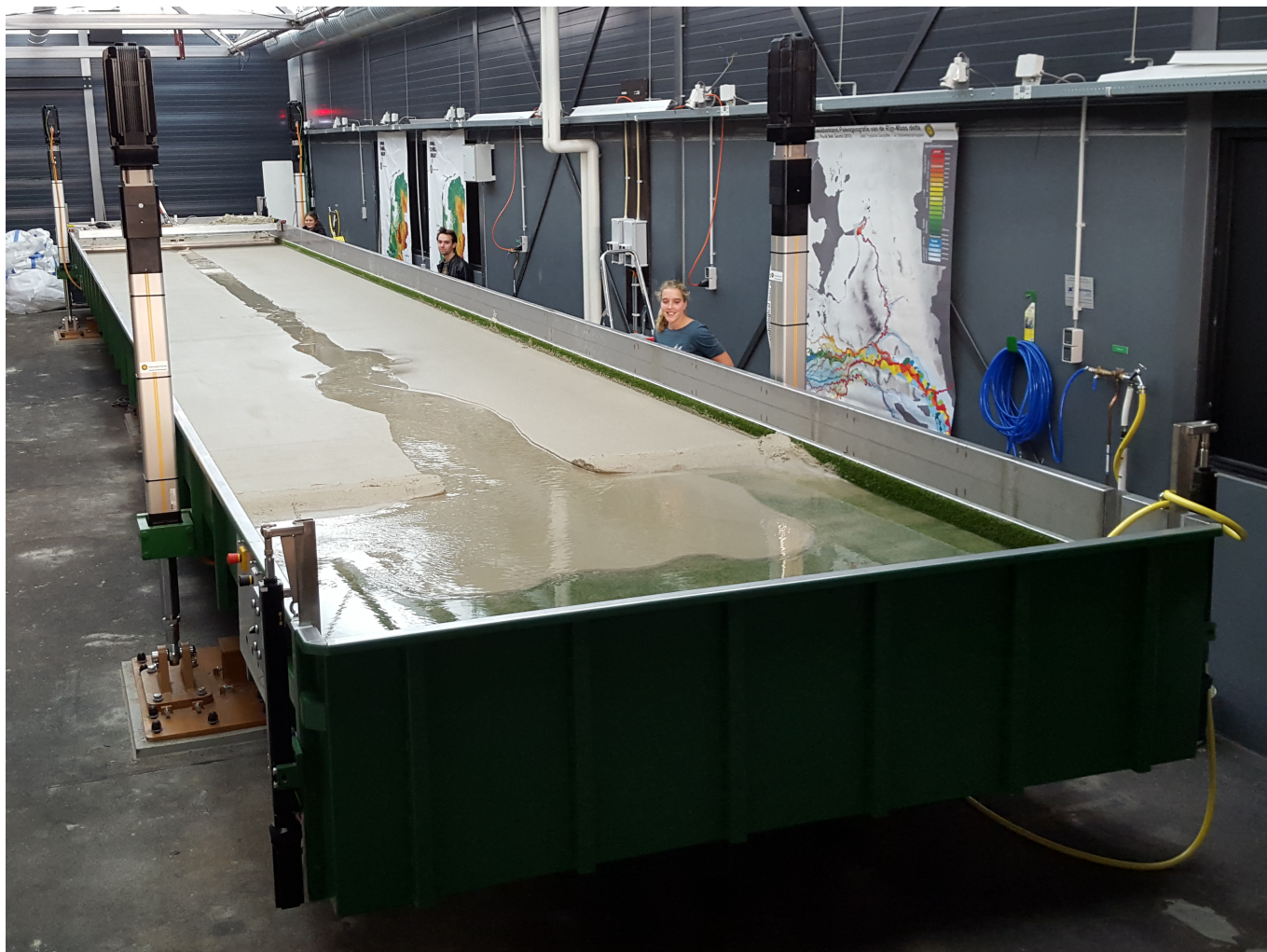
Figure 2. The Metronome tidal facility. Note PhD candidates for scale. The flume floor below the sand is covered in artificial grass (see text). Note the vertically mounted actuators that drive the flow. This pilot experiment started as a 0.2 m by 0.03 m straight initial channel and ran for about 12 hours with a slope amplitude of 0.005 m/m and a period of 30 s and 100 L/hr river inflow.
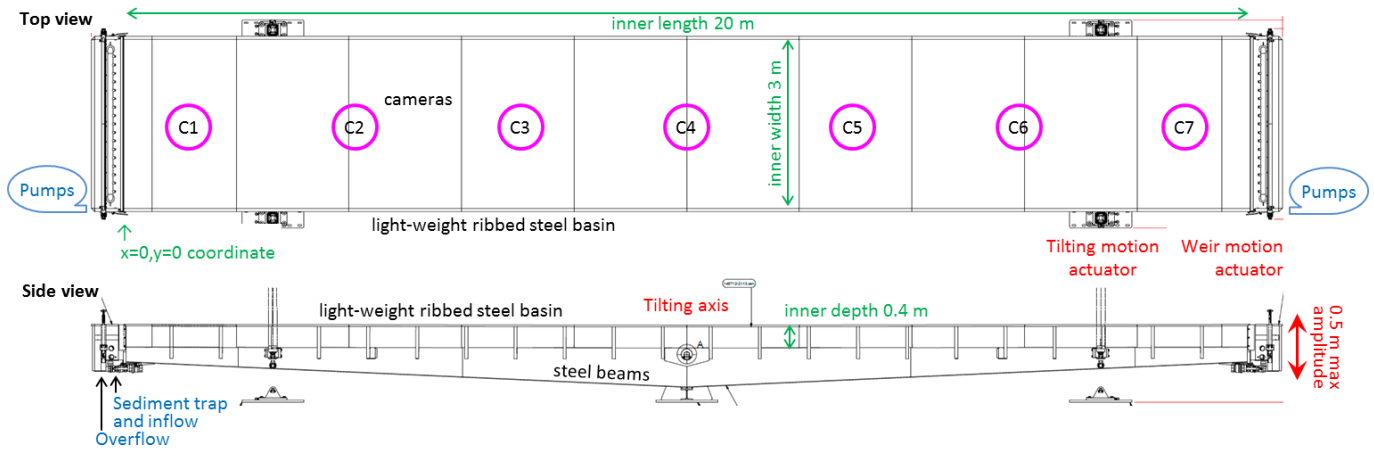
Figure 3. Geometry of the Metronome facility. The inner basin measures 20.00 m in length 3.00 m in width and 0.40 m in depth and the maximum tilting amplitude is 0.5 m at the end tank resulting in a tilting slope amplitude of 0.05 m/m. Both flume ends have end tanks with a 0.3 m long stilling basin functioning as sediment trap and pumped water inflow, separated by an automated weir from the outside 0.2 m long overflow basin with a 2 mm mesh to capture PIV particles. Motion is controlled by four 20 kN actuators for tilting and two small actuators for each end tank weir. Cameras C1–7 are mounted 3.7 m above the flume floor.
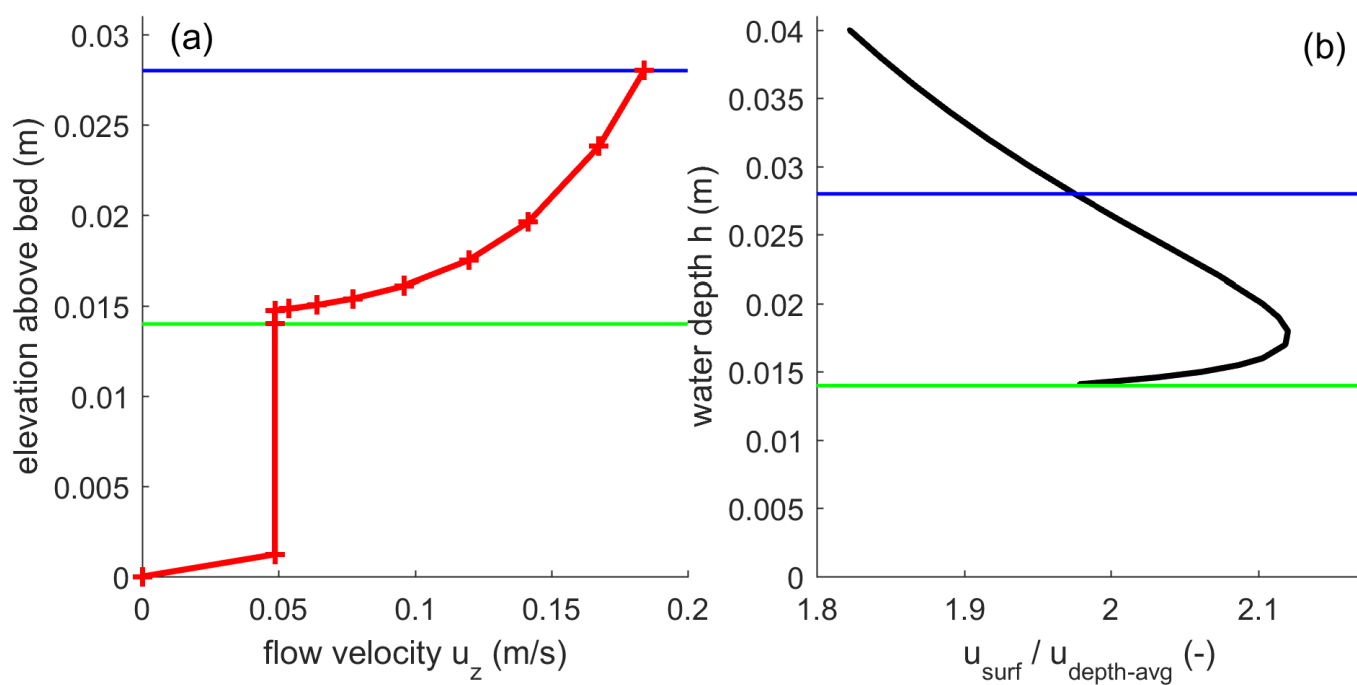
Figure 4. Application of the Baptist et al. (2006) vegetation friction relation to the artificial vegetation in the Metronome. (a) Flow velocity profile (red) between the bed and the water surface (blue). Height of vegetation indicated in green. (b) Ratio between water surface velocity u_{surf} and depth-averaged velocity $u_{depth-avg}$ as a function of total flow depth. This is independent of slope. Given the insensitivity to water depth variations, a constant value of 1.95 is assumed for comparison of measured and modelled flow velocities.
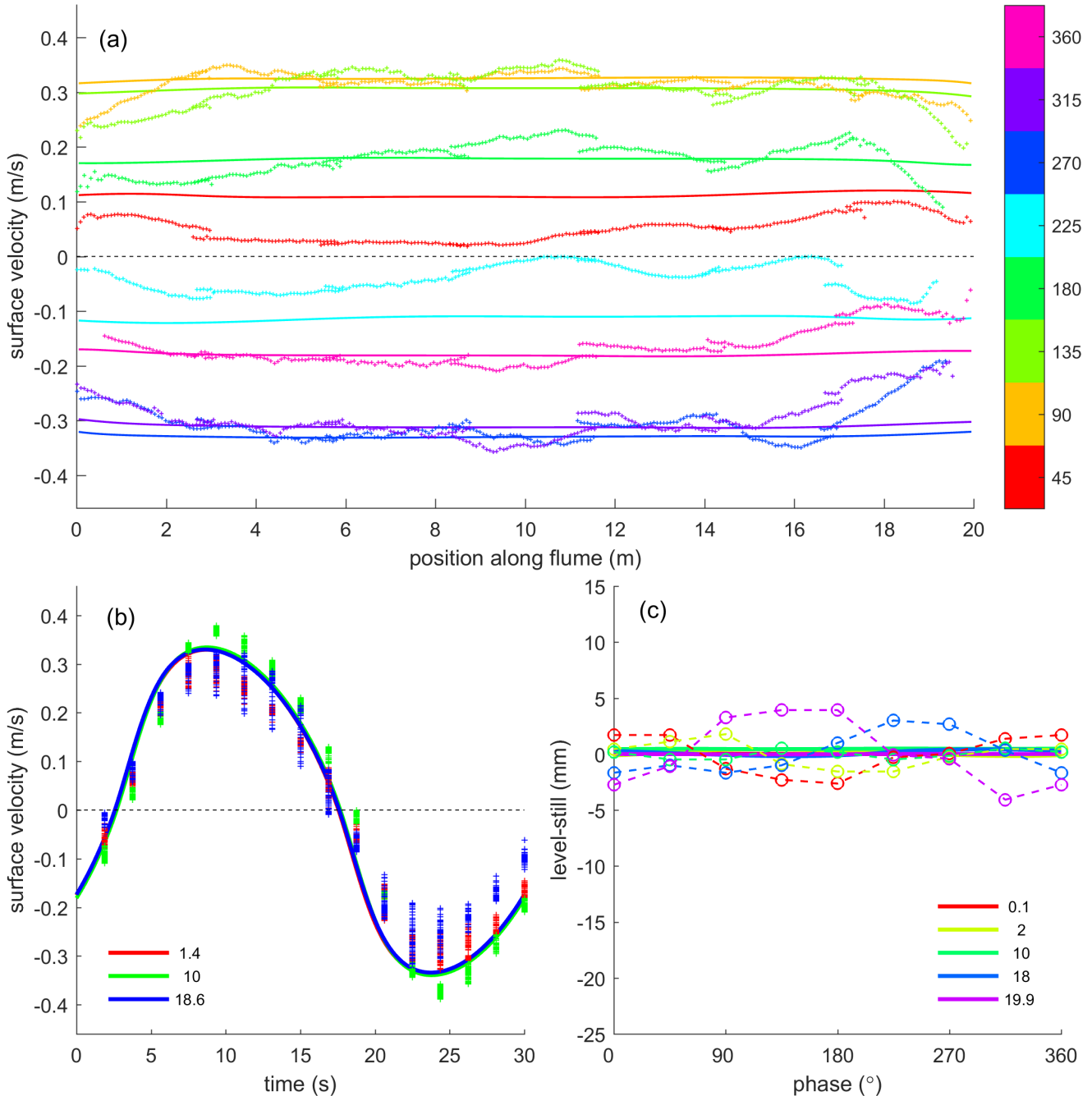
Figure 5. Flow data from PIV and modelled flow with 30 s period tilting at 0.009 m/m slope amplitude with both boundaries open. (a) Flow velocity at the water surface along the flume for selected phases of the tidal cycle. (b) Flow velocity at the water surface in one tidal cycle for selected positions along the flume measured from $x = 0$ m, indicated in legend. (c) Water level as a function of phase in the tidal cycle for selected positions along the flume. Measured water levels have correct amplitude and phase but possibly erroneous vertical offsets. Data are plotted as symbols and model results are plotted as drawn lines.
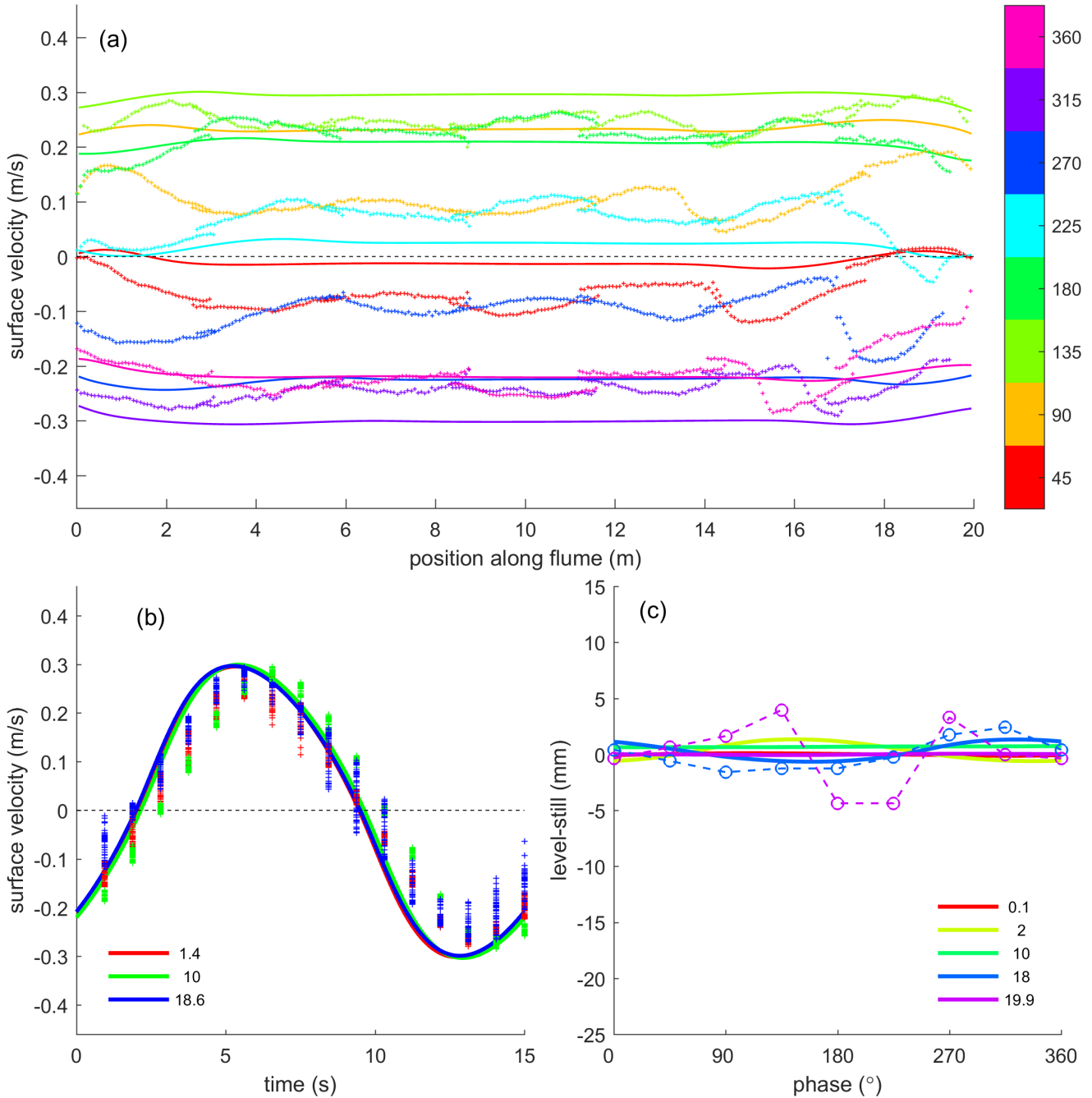
Figure 6. Flow data from PIV and modelled flow with 15 s period tilting at 0.009 m/m slope amplitude with both boundaries open. (a) Flow velocity at the water surface along the flume for selected phases of the tidal cycle. (b) Flow velocity at the water surface in one tidal cycle for selected positions along the flume measured from $x = 0$ m, indicated in legend. (c) Water level as a function of phase in the tidal cycle for selected positions along the flume. Measured water levels have correct amplitude and phase but possibly erroneous vertical offsets. Data are plotted as symbols and model results are plotted as drawn lines.
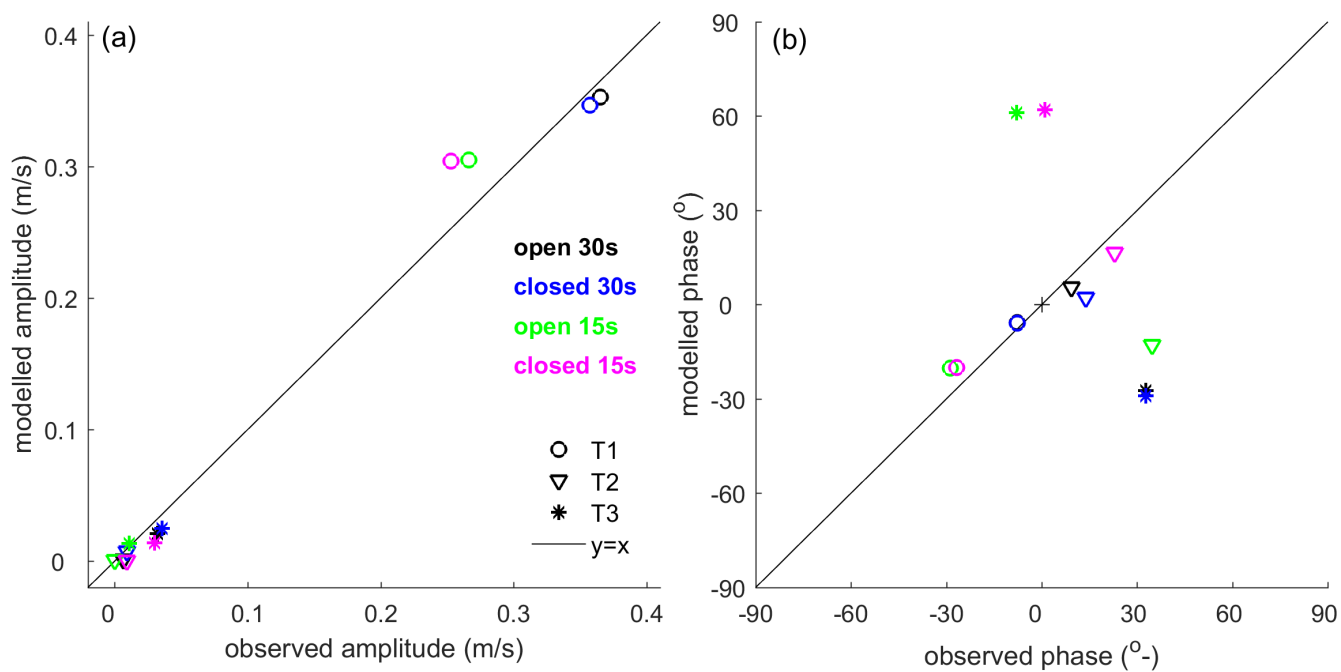
Figure 7. Tidal amplitude (a) and phase (b) in the velocity signal of the model runs compared to the experiments for the tilting flume. The principal tide 'T1' is the full tidal period of 30 s or 15 s and the first overtide 'T2' and second overtide 'T3' the higher harmonics. Dashed lines indicate the perfect fit plus or minus an error of 0.01 m/s to indicate the uncertainty range of the data.
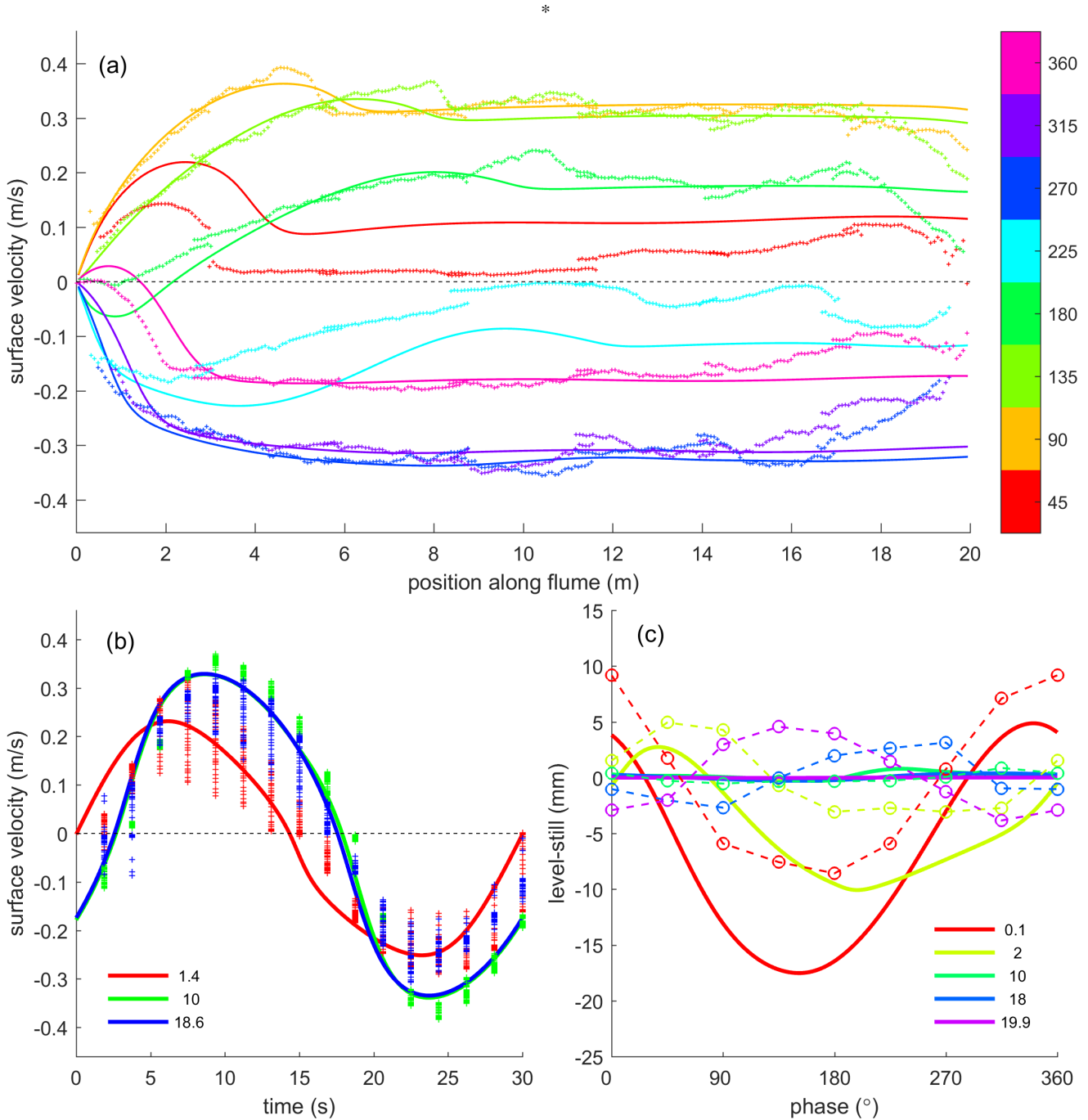
Figure 8. Flow data from PIV and modelled flow with 30 s period tilting at 0.009 m/m slope amplitude with upstream boundary closed. (a) Flow velocity at the water surface along the flume for selected phases of the tidal cycle. (b) Flow velocity at the water surface in one tidal cycle for selected positions along the flume measured from $x = 0$ m, indicated in legend. (c) Water level as a function of phase in the tidal cycle for selected positions along the flume. Measured water levels have correct amplitude and phase but possibly erroneous vertical offsets. Data are plotted as symbols and model results are plotted as drawn lines.
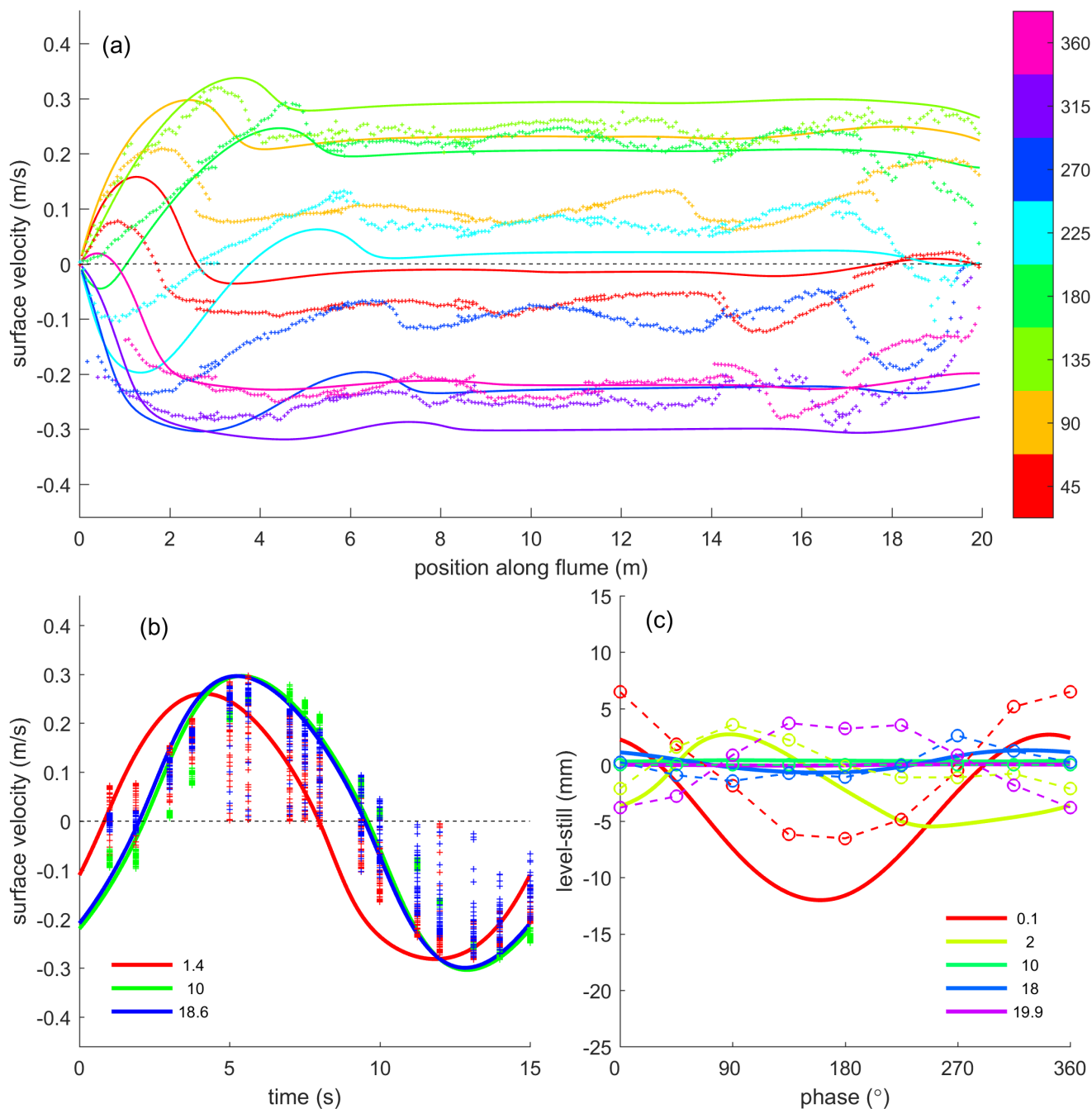
Figure 9. Flow data from PIV and modelled flow with 15 s period tilting at 0.009 m/m slope amplitude with upstream boundary closed. (a) Flow velocity at the water surface along the flume for selected phases of the tidal cycle. (b) Flow velocity at the water surface in one tidal cycle for selected positions along the flume measured from $x = 0$ m, indicated in legend. (c) Water level as a function of phase in the tidal cycle for selected positions along the flume. Measured water levels have correct amplitude and phase but possibly erroneous vertical offsets. Data are plotted as symbols and model results are plotted as drawn lines.
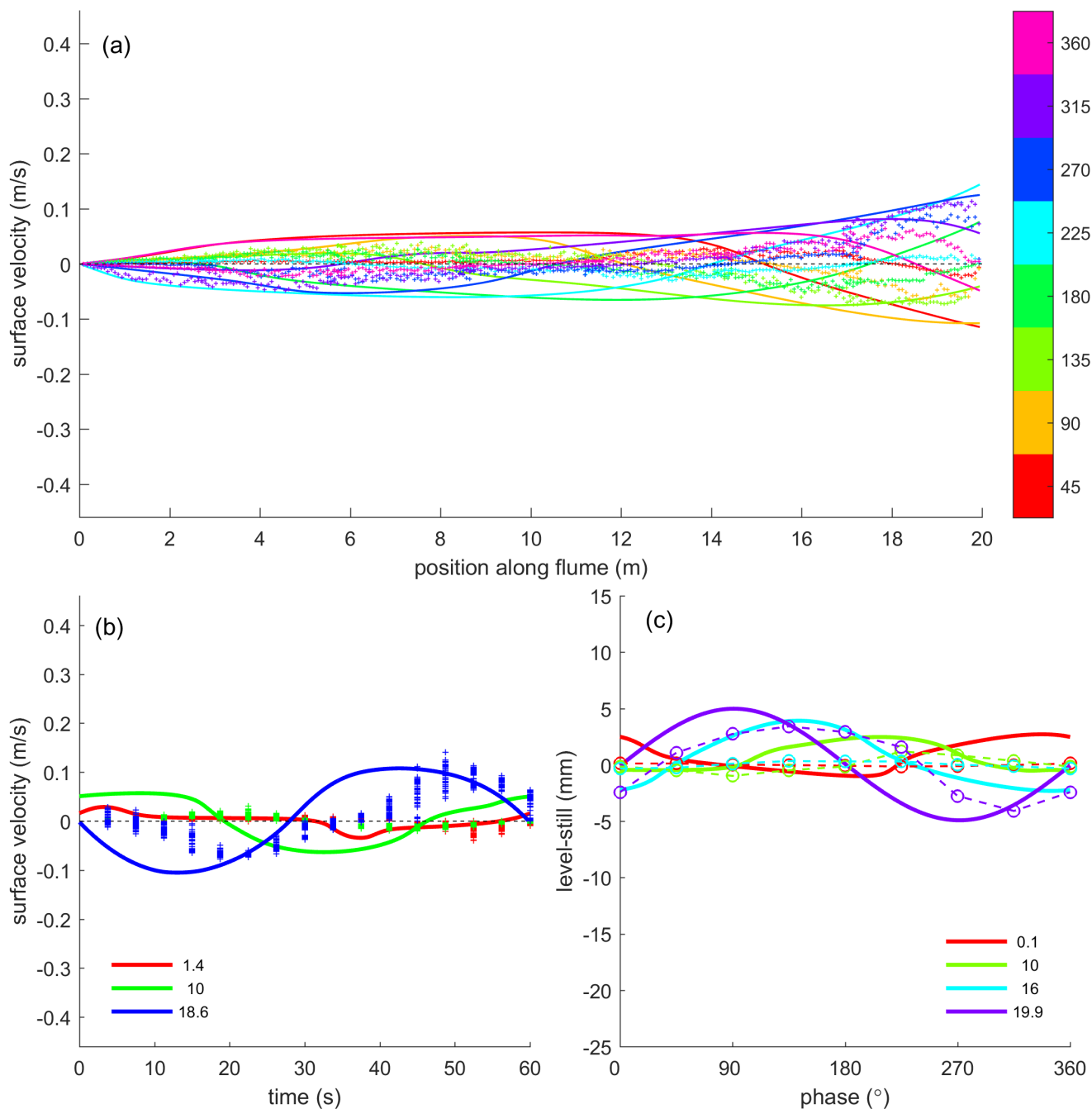
Figure 10. Flow data from PIV and modelled flow with 60 s period sealevel fluctuation at 0.01 m amplitude with the landward boundary closed. Positive flow velocity is in the ebb direction. (a) Flow velocity at the water surface along the flume for selected phases of the tidal cycle. (b) Flow velocity at the water surface in one tidal cycle for selected positions along the flume measured from $x = 0$ m, indicated in legend. (c) Water level as a function of phase in the tidal cycle for selected positions along the flume, indicated in the legend. Measured water levels have correct amplitude and phase but possibly erroneous vertical offsets. Data are plotted as symbols and model results are plotted as drawn lines.
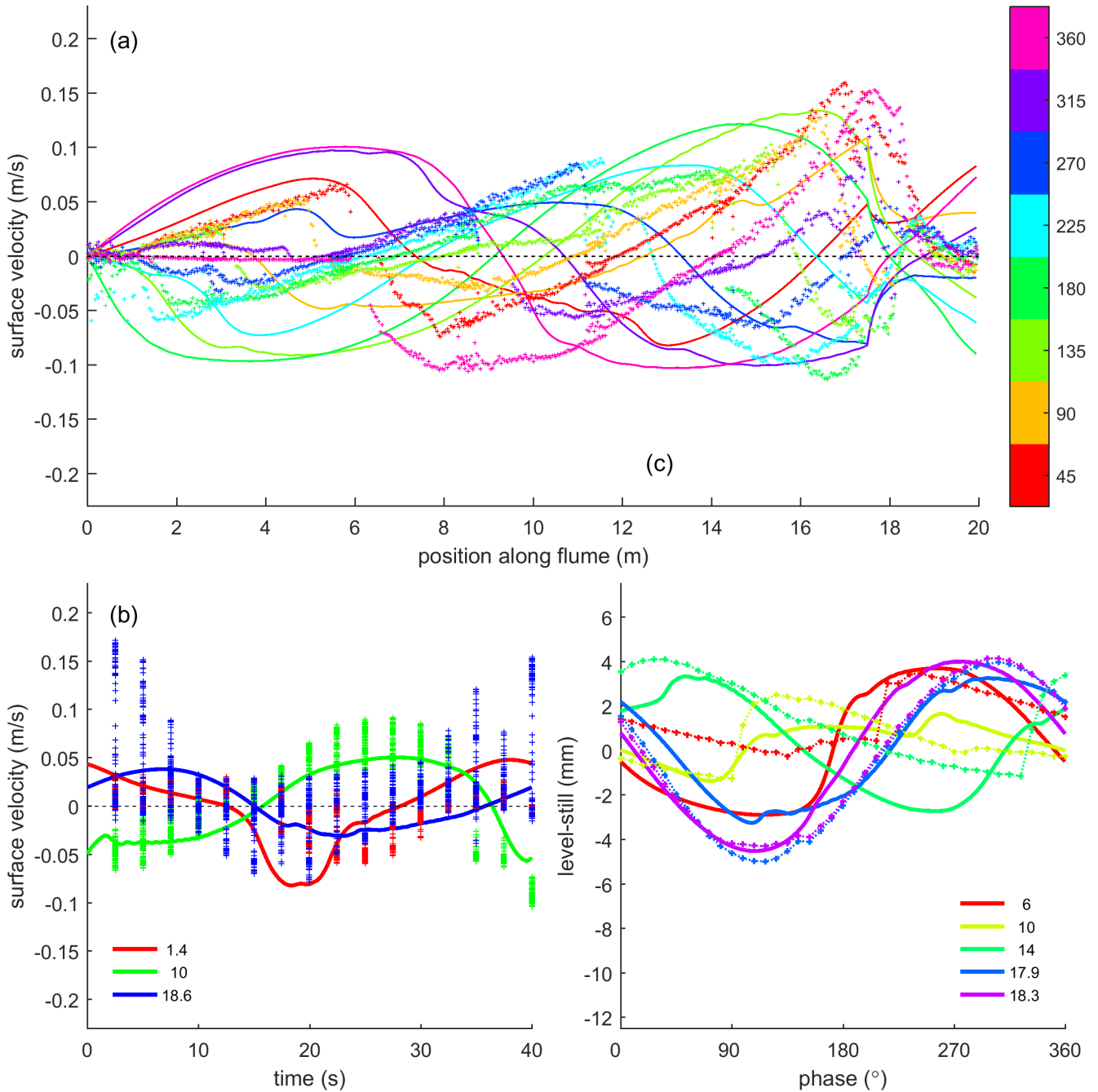
Figure 11. Flow data in an 18 m sand-bed channel with a 2 m long by 3 m wide sea from PIV and modelled flow with 40 s period sealevel fluctuation of 0.007 m amplitude with the landward boundary closed. Note that the vertical axis range is half that of the tilting experiment. (a) Flow velocity at the water surface along the flume for selected phases of the tidal cycle. (b) Flow velocity at the water surface in one tidal cycle for selected positions along the flume measured from $x = 0$ m, indicated in legend. (c) Water level measured by acoustics as a function of phase in the tidal cycle for selected positions along the flume. Data are plotted as symbols and model results are plotted as drawn lines.
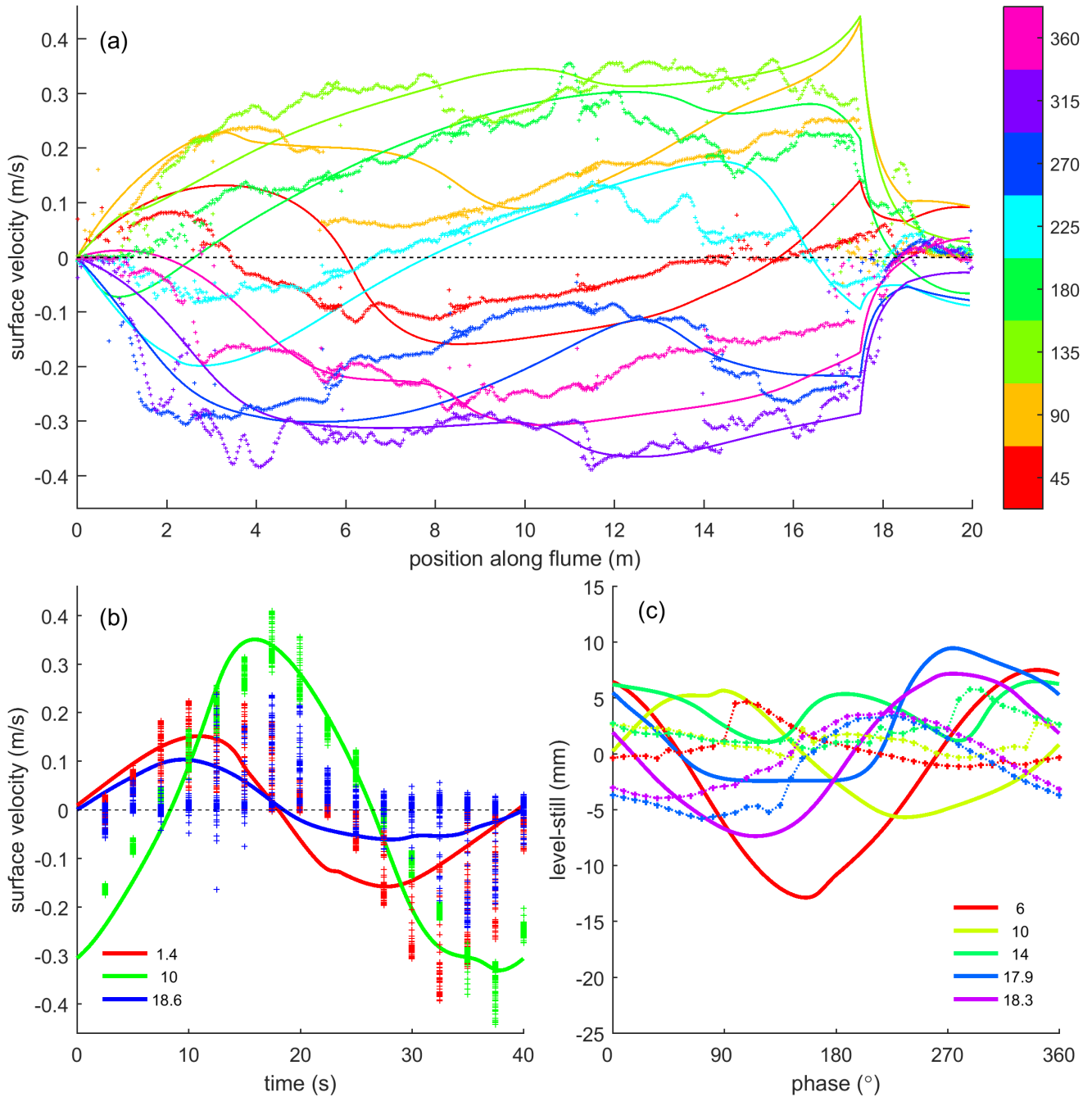
Figure 12. Flow data in an 18 m sand-bed channel with a 2 m long by 3 m wide sea from PIV and modelled flow with 40 s period tilting at 0.004 m/m slope amplitude with the landward boundary closed. (a) Flow velocity at the water surface along the flume for selected phases of the tidal cycle. (b) Flow velocity at the water surface in one tidal cycle for selected positions along the flume measured from $x = 0$ m, indicated in legend. (c) Water level measured by acoustics as a function of phase in the tidal cycle for selected positions along the flume. Data are plotted as symbols and model results are plotted as drawn lines.
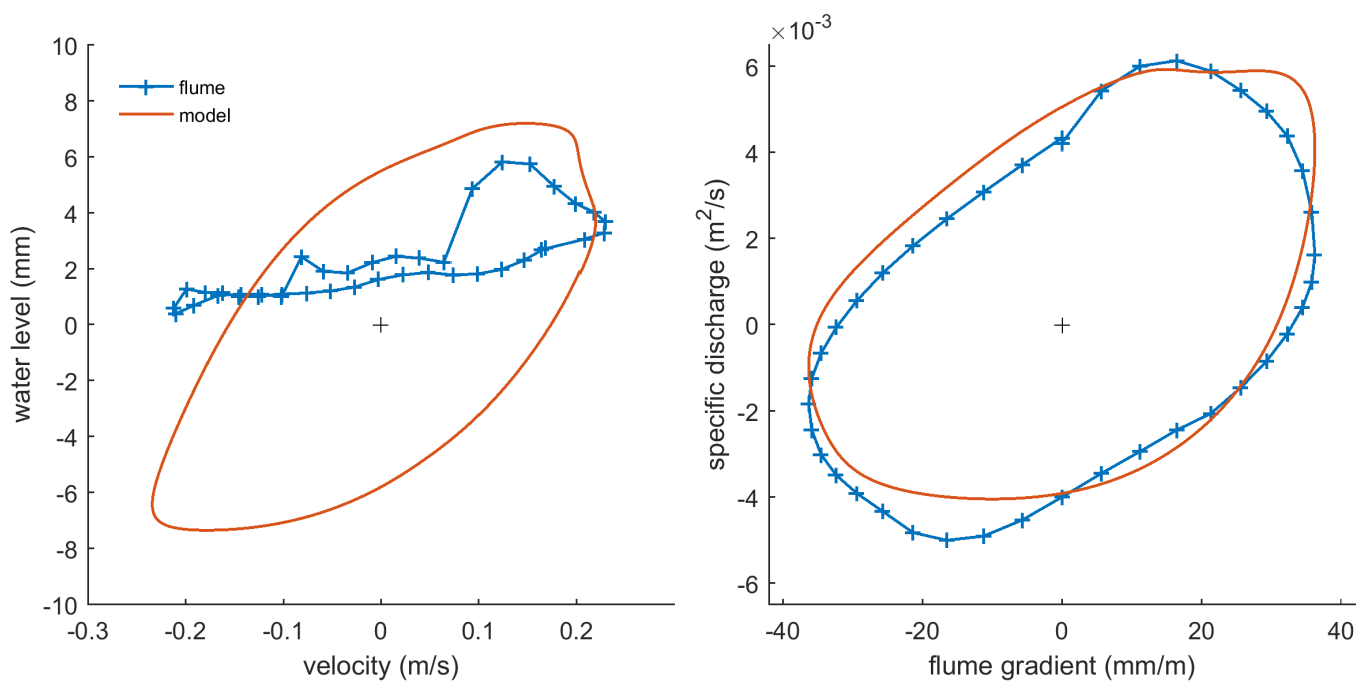
Figure 13. Hysteresis of flux and water level relative to still water in one tidal cycle in the tilting sand-bed experiment at $x = 10$ m. (a) Water level fluctuation against depth-averaged flow velocity. (b) Specific discharge against tilting flume gradient.
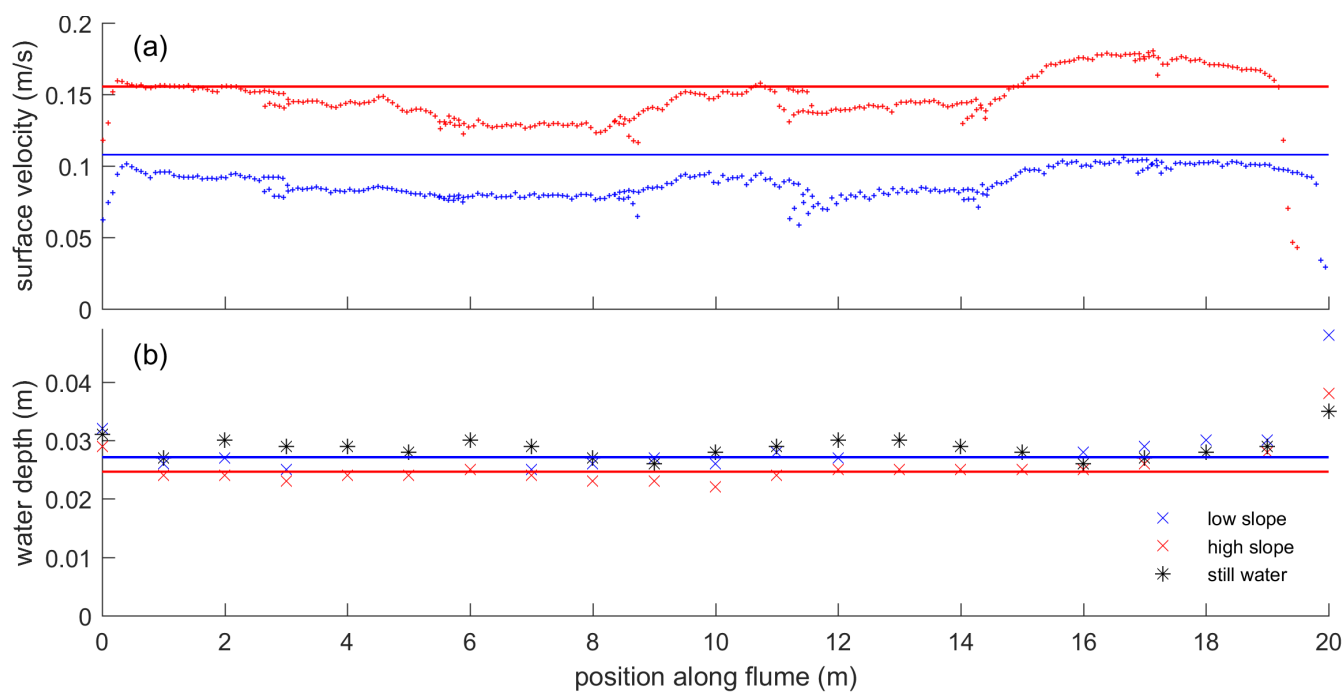
Figure 14. Unidirectional flow data from PIV for the constant low slope and high slope experiments. (a) Flow velocity at the water surface along the flume. Drawn lines are analytically calculated surface flow velocities. (b) Approximate water depths measured for both experiments. Drawn lines are average values used in flow calculation. Still water depth measurements show variation of bed level due to irregularities in artificial grass height and sand layer thickness at the bottom of the grass. Flow velocity is defined as positive in the ebb-direction with $x = 0$ m being the upstream boundary.
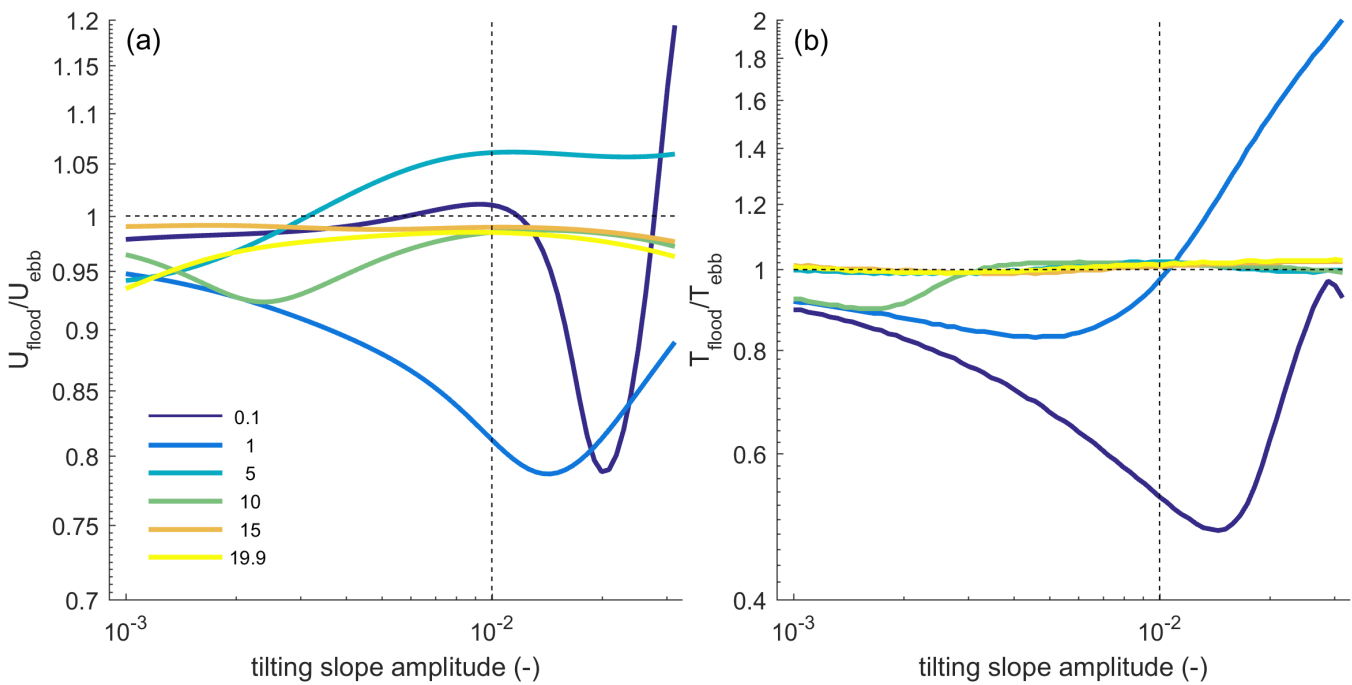
Figure 15. Modelled tidal asymmetry for increasing tilting slope amplitude with 30 s period. (a) Velocity asymmetry indicating potential sediment importing or exporting tendency. (b) Duration asymmetry between peak flow velocities as indicative of slack duration. Legend indicates position in the Metronome from upstream closed boundary to the open boundary. Horizontal dashed lines indicate symmetry and vertical dashed lines indicate a typical slope in 2 cm deep experiments with mobile sediment.
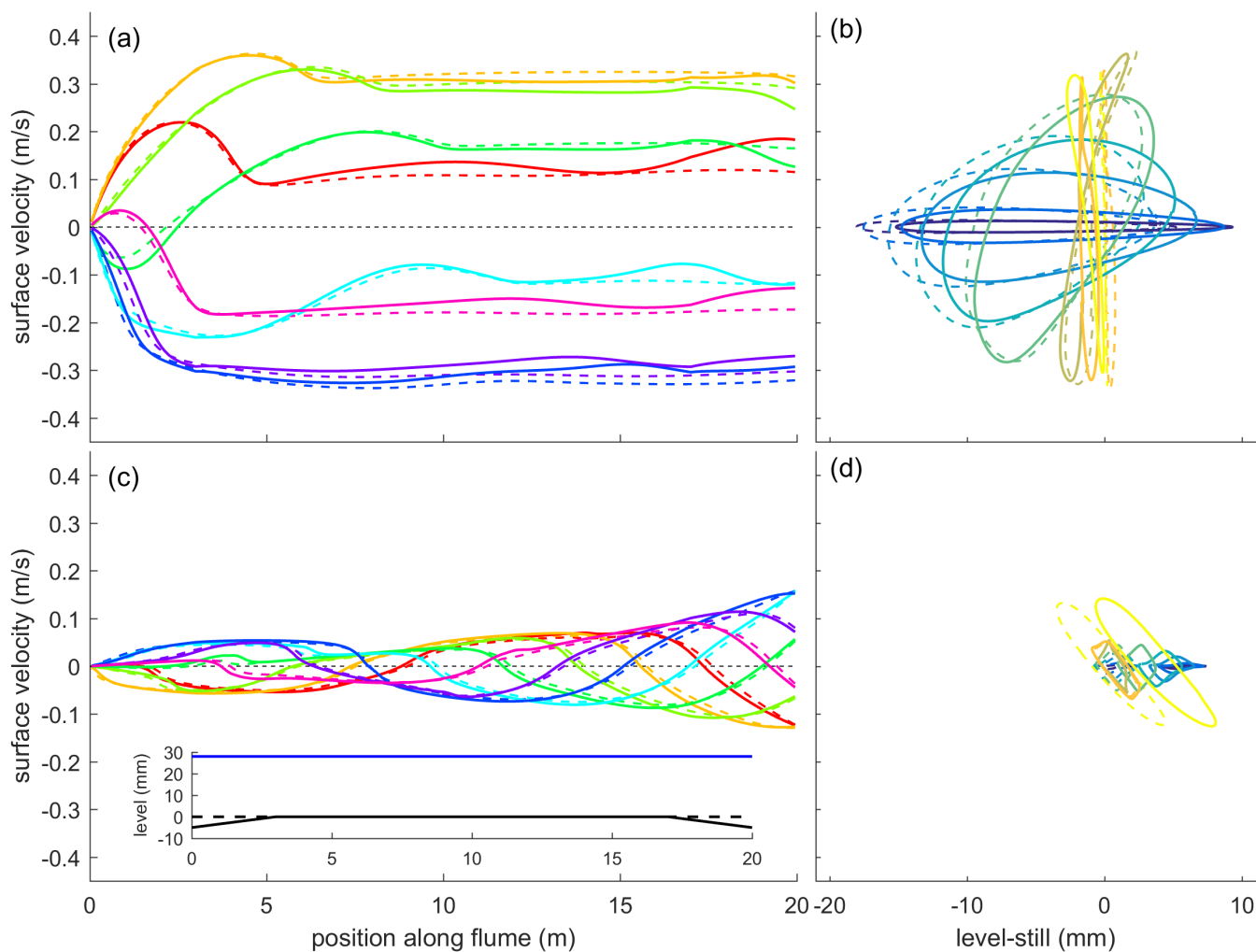
Figure 16. Sensitivity of flow to depth variation in the basin (drawn lines) compared with the ideal depth (dashed lines) for 30 s period model runs. Inset in (c) shows modified bed elevation. Runs with original depth are same as in Fig. 8. (a,c) Flow velocity at the water surface along the flume for selected phases of the tidal cycle. Legend as in Fig. 8. (b,d) Water level and flow velocity in one tidal cycle showing hysteresis. Legend as in Fig. 13. (a,b) Tilting at 0.09 m amplitude with upstream boundary closed. (c,d) Reynolds method with sealevel fluctuation at 0.01 m amplitude with the landward boundary closed.
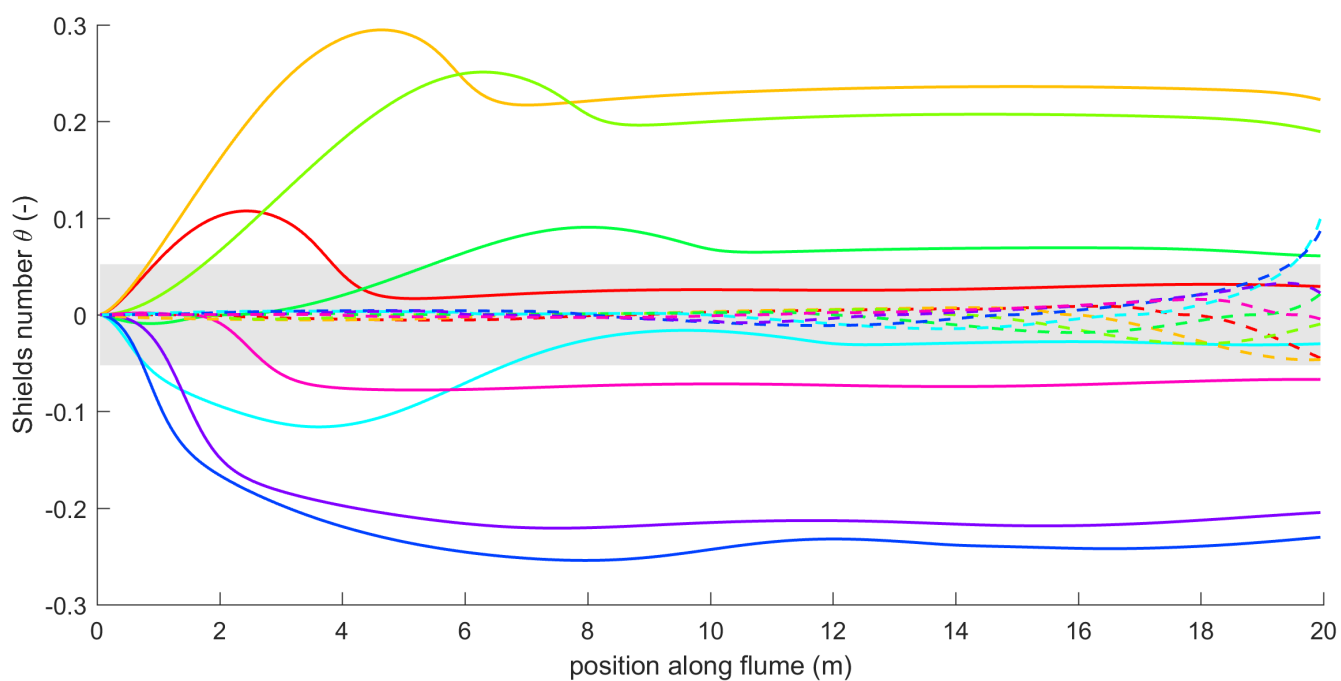
Figure 17. Sediment mobility calculated for tidal flows driven by periodic tilting (drawn lines) and by the Reynolds method with periodic sea surface fluctuation (dashed lines). Legend as in Fig. 8. Gray area indicates immobile sediment.